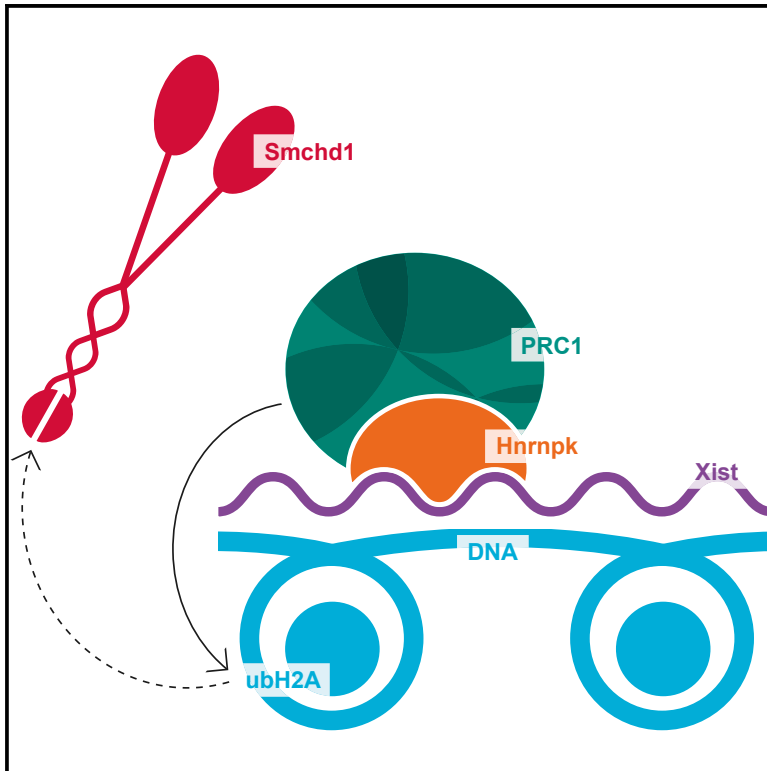


Cell Reports

Smchd1 Targeting to the Inactive X Is Dependent on the *Xist*-HnrnpK-PRC1 Pathway

Graphical Abstract



Authors

Natasha Jansz, Tatyana Nesterova, Andrew Keniry, ..., Neil Brockdorff, James M. Murphy, Marnie E. Blewitt

Correspondence

blewitt@wehi.edu.au

In Brief

Jansz et al. report that the chromatin protein Smchd1 depends on polycomb repressive complex 1-mediated ubiquitylation of histone H2A for its recruitment to the inactive X chromosome and for its protein stability. These data have implications for Smchd1 targeting genome-wide.

Highlights

- Smchd1 does not bind endogenous RNA with detectable sequence specificity
- Smchd1 depends on the *Xist*-HnrnpK-PRC1 pathway for recruitment to the inactive X
- Smchd1 depends on histone H2A lysine 119 ubiquitination for inactive X localization
- Smchd1 protein stability depends on histone H2A lysine 119 ubiquitination



Jansz et al., 2018, Cell Reports 25, 1912–1923
November 13, 2018 © 2018 The Author(s).
<https://doi.org/10.1016/j.celrep.2018.10.044>

CellPress

Smchd1 Targeting to the Inactive X Is Dependent on the *Xist*-HnnpK-PRC1 Pathway

Natasha Jansz,^{1,2} Tatyana Nesterova,³ Andrew Keniry,^{1,2} Megan Iminoff,¹ Peter F. Hickey,^{1,2} Greta Pintacuda,³ Osamu Masui,⁴ Simon Kobelke,⁵ Niall Geoghegan,^{1,2} Kelsey A. Breslin,¹ Tracy A. Willson,¹ Kelly Rogers,^{1,2} Graham F. Kay,⁶ Archa H. Fox,⁵ Haruhiko Koseki,⁴ Neil Brockdorff,³ James M. Murphy,^{1,2} and Marnie E. Blewitt^{1,2,7,8,*}

¹The Walter and Eliza Hall Institute of Medical Research, 1G Royal Parade, Parkville, Melbourne, VIC 3052, Australia

²Department of Medical Biology, University of Melbourne, Melbourne, VIC 3010, Australia

³Developmental Epigenetics, Department of Biochemistry, University of Oxford, South Parks Road, Oxford OX1 3QU, UK

⁴Centre for Integrative Medical Sciences, RIKEN Yokohama Institute, 1-7-22, Suehiro-cho, Tsurumi, Yokohama, Kanagawa 230-0045, Japan

⁵School of Human Sciences, The University of Western Australia, Crawley, WA 6009, Australia

⁶QIMR Berghofer Medical Research Institute, Brisbane, QLD, Australia

⁷Department of Genetics, University of Melbourne, Melbourne, VIC 3010, Australia

⁸Lead Contact

*Correspondence: blewitt@wehi.edu.au

<https://doi.org/10.1016/j.celrep.2018.10.044>

SUMMARY

We and others have recently reported that the SMC protein Smchd1 is a regulator of chromosome conformation. Smchd1 is critical for the structure of the inactive X chromosome and at autosomal targets such as the *Hox* genes. However, it is unknown how Smchd1 is recruited to these sites. Here, we report that Smchd1 localizes to the inactive X via the *Xist*-HnnpK-PRC1 (polycomb repressive complex 1) pathway. Contrary to previous reports, Smchd1 does not bind *Xist* or other RNA molecules with any specificity. Rather, the localization of Smchd1 to the inactive X is H2AK119ub dependent. Following perturbation of this interaction, Smchd1 is destabilized, which has consequences for gene silencing genome-wide. Our work adds Smchd1 to the PRC1 silencing pathway for X chromosome inactivation.

INTRODUCTION

X chromosome inactivation (XCI) is an epigenetic process that has evolved in mammals to ensure equal dosage of X-linked genes between male and female cells (Lyon, 1961). During development, XCI is initiated by upregulation of the long non-coding RNA (lncRNA) *Xist* from the allele on the future inactive X chromosome (Xi) (Brockdorff et al., 1992; Brown et al., 1991; Kay et al., 1993; Penny et al., 1996). *Xist* coats the Xi *in cis* and elicits a cascade of repressive events that result in the establishment of gene silencing that is stably maintained during the lifetime of the female mammal. It is this stable maintenance of silencing through mitosis, independent of any genetic change on the Xi, that defines this process as epigenetic.

The precise mechanisms by which the expression of an lncRNA can mediate chromosome-wide gene silencing has been the focus of much research. *Xist* is thought to elicit gene silencing via direct or indirect recruitment of a series of proteins

that mediate changes to the chromatin. However, precisely how each factor fits into the hierarchy of XCI and how they mediate gene silencing have not always been clear. A good example of this has been for the polycomb group proteins (Brockdorff, 2017). Originally, polycomb repressive complex 2 (PRC2) was reported to bind the A-repeat of *Xist* (Zhao et al., 2008), and it was believed that the PRC2 mark H3K27me3 then enabled PRC1 binding via the canonical polycomb recruitment model (Cao et al., 2002). However, it has more recently become clear that instead, the B-repeat of *Xist* recruits non-canonical PRC1 (Almeida et al., 2017) via direct binding to HnnpK (Pintacuda et al., 2017). The PRC1 mark H2AK119ub subsequently enables recruitment of PRC2 and canonical PRC1.

In 2015, four landmark studies identified novel protein interactors of *Xist* through high-throughput screening approaches (McHugh et al., 2015; Minajigi et al., 2015; Moindrot et al., 2015; Monfort et al., 2015). Characterization of select candidate interactors have identified new pathways for *Xist*-mediated gene silencing and revealed some of the earliest factors that are required to inhibit transcription. The screen by Minajigi and colleagues was performed in fibroblasts and identified 200 proteins that were enriched for *Xist* binding 2-fold over background. This list of proteins included the epigenetic modifier structural maintenance of chromosomes hinge domain containing 1 (Smchd1) (Minajigi et al., 2015).

Smchd1 is a non-canonical structural maintenance of chromosomes (SMC) family protein that is critically involved in both random and imprinted XCI during development; female embryos that develop in the absence of Smchd1 do not survive beyond mid-gestation (Blewitt et al., 2008). In these embryos, upregulation of gene expression from the Xi is accompanied by DNA hypomethylation (Blewitt et al., 2008; Gendrel et al., 2012, 2013; Mould et al., 2013); however, the function of Smchd1 in XCI had remained elusive. We and others have very recently found that Smchd1 plays an important structural role on the Xi. This is achieved by insulating the Xi from epigenetic modifiers that mediate long-range chromatin interactions, to contribute to the unique higher-order conformation of the Xi (Gdula et al., 2018; Jansz et al., 2018; Wang et al., 2018).



One major open question is how Smchd1 is targeted to the chromatin of the Xi. Mouse and human SMCHD1 bind broadly over the Xi, covering both H3K9me3-enriched gene-poor regions and gene-rich H3K27me3-*Xist* domains (Gdula et al., 2018; Jansz et al., 2018; Nozawa et al., 2013; Wang et al., 2018). It has been proposed that targeting of Smchd1 to H3K9me3-enriched chromatin is mediated by a direct protein-protein interaction between Smchd1 and Lr1f1 (HBIx1 in humans) (Nozawa et al., 2013). The Smchd1-Lr1f1 complex preferentially binds Hp1 γ , which in turn binds to H3K9me2 and H3K9me3 through its chromodomain. While the interaction between Lr1f1 and Smchd1 exists on the Xi, Smchd1 remains enriched over the Xi territory when this interaction is perturbed (Brideau et al., 2015). This suggests that there is an alternative mechanism by which Smchd1 is targeted to the Xi. Moreover, this pathway cannot fully explain Smchd1 targeting to autosomes, given that several Smchd1 targets, such as the *Hox* genes, are not decorated by H3K9 methylation but are strongly enriched for Smchd1 (Chen et al., 2015; Jansz et al., 2018).

SMCHD1 localizes to the Xi in an *XIST*-dependent manner in both humans and mice, and Smchd1 was identified as a candidate *Xist* interacting partner in fibroblasts (Minajigi et al., 2015; Nozawa et al., 2013; Wang et al., 2018). Furthermore, we have previously shown that the hinge domain of Smchd1 has the capacity to bind RNA oligonucleotides *in vitro* (Chen et al., 2015). Therefore, we investigated the interaction between Smchd1 and *Xist* during the maintenance of XCI. We found that while Smchd1 shows a dependency on *Xist* for its localization to the Xi in mice, it is not due to a direct RNA-protein interaction. Rather, we found that Smchd1 localization to the Xi is dependent on the newly identified *Xist*-HnrnpK-PRC1 pathway. Consistent with this, we found that Smchd1 recruitment during the establishment of XCI requires the *Xist* B-repeat. Furthermore, we show PRC1-associated Ring1A/B activity is required for Smchd1 stability, meaning that this pathway is necessary for Smchd1-mediated gene silencing genome-wide.

RESULTS

Smchd1 Localization to the Xi in Mice Is Dependent on *Xist*

We have previously described an *Smchd1*^{GFP} knockin allele, which produces a functionally wild-type Smchd1-GFP fusion protein (Jansz et al., 2018). In female cells homozygous for this allele, Smchd1-GFP appears as a bright nuclear focus, co-localizing with the Xi marker H2AK119ub (Jansz et al., 2018). To determine whether Smchd1-GFP localization to the Xi is *Xist* dependent in interphase nuclei, we directly displaced *Xist* from the Xi using an antisense locked nucleic acid (LNA) probe to a region downstream of the C-repeat of *Xist*, which is important for its *cis* localization to the Xi (Sarma et al., 2010) in immortalized female *Smchd1*^{GFP/GFP} mouse embryonic fibroblasts (MEFs). Cells were subject to live cell imaging 3 hr post-transfection, allowing us to visualize several cells specifically when the probe entered the nucleus and the subsequent loss of focal Smchd1 enrichment with the LNA-4978 (Video S1), but not the scrambled control (Video S2). Transfection with LNA-4978 resulted in only 21% of cells possessing an

Smchd1-GFP focus, compared with 82% of cells transfected with a scrambled control (Figure 1A). This suggests that the continuous enrichment of Smchd1 on the Xi in interphase nuclei is dependent on *Xist*.

Alongside transient live cell imaging experiments, we used small hairpin RNAs (shRNAs) to stably knock down the HBIx homolog Lr1f1 and the nuclear matrix protein HnrnpU (Figure S1). HBIx has been proposed to interact with SMCHD1 on the Xi in humans, and HnrnpU is required for the *cis* localization of *Xist* to the Xi in certain cellular contexts (Hasegawa et al., 2010; Kolpa et al., 2016; Nozawa et al., 2013). Lr1f1 knockdown did not affect Smchd1 localization in either immortalized MEFs or primary neural stem cells (NSCs), consistent with previous reports (Brideau et al., 2015). By contrast, knock down of *HnrnpU* in immortalized *Smchd1*^{GFP/GFP} MEFs resulted in only 16% of cells possessing Smchd1-GFP foci when compared to 83% in non-silencing controls (Figure 1B). *HnrnpU* knockdown did not result in the loss of Smchd1-GFP Xi localization in primary NSCs (Figure 1B); however, it is known that the dependency of *Xist* on HnrnpU is cell type specific, and neural cells do not require HnrnpU for *Xist* localization (Kolpa et al., 2016). We therefore performed *Xist* RNA fluorescence *in situ* hybridization (FISH) in primary NSCs and, as expected based on the study by Kolpa et al. (2016), we found that knock down of HnrnpU did not result in a loss of focal *Xist* enrichment in this context (Figure 1C). The differing dependency between NSCs and MEFs on HnrnpU for *Xist* localization was helpful in this instance, as it provided additional support that the Xi localization of Smchd1 is dependent on *Xist* rather than on HnrnpU. *Smchd1* expression was not altered upon *HnrnpU* knockdown (Figure S1), nor did HnrnpU co-immunoprecipitate with Smchd1-GFP (Figure 1D), indicating that the loss of Smchd1-GFP from the Xi is not a consequence of either reduced protein levels or a direct protein-protein interaction with HnrnpU. Therefore, displacing *Xist* from the Xi, either indirectly or directly, results in loss of Smchd1-GFP focal enrichment in the nucleus. These data suggest that in mice, Smchd1-GFP Xi localization is *Xist* RNA dependent, which is consistent with a very recent study (Wang et al., 2018).

Smchd1 Does Not Bind to Endogenous RNA Genome-wide with Sequence Specificity

We wanted to investigate whether Smchd1 directly interacts with *Xist* and other RNA molecules genome-wide. We used photoactivatable ribonucleoside-enhanced crosslinking and immunoprecipitation (PAR-CLIP), which uses the photoactivatable uridine analog 4-thiouridine (4-SU) to selectively crosslink proteins to nucleic acids (Hafner et al., 2010). Our protocol also incorporated multiple stringent purification steps, including a DNase digest to prevent DNA-mediated RNA immunoprecipitation and partial T1 RNase digest to disrupt large riboprotein complexes and minimize the detection of indirect interactions (Figure S2).

PAR-CLIP conditions were optimized to ensure robust enrichment and retention of Smchd1-GFP throughout all stages of the protocol, while minimizing non-specific contamination of other ribonucleoproteins (Figure S2). To ensure that we had the capacity to enrich for RNA following modifications to the protocol, the optimized protocol was used on cells expressing

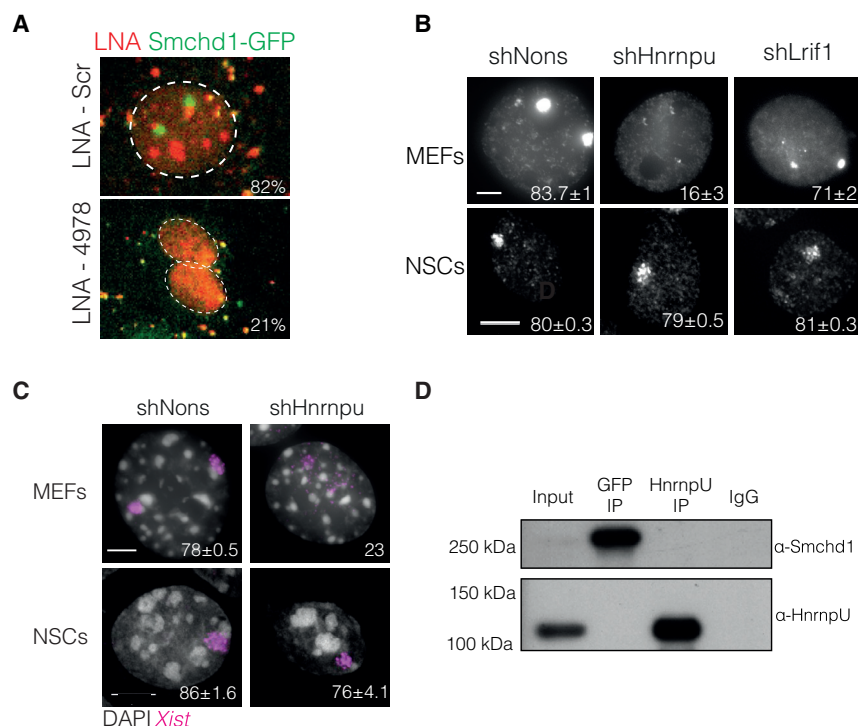


Figure 1. Smchd1 Localization to the Xist Dependent

(A) Screenshot from live cell imaging experiment performed in immortalized female *Smchd1*^{GFP/GFP} MEFs following transfection with either a scrambled LNA probe or one antisense for Xist. Smchd1-GFP (green) and LNA (red). Nuclei are outlined in white. Punctate distribution of LNA probe in the cells is lysosomal uptake of the oligonucleotides following transfection. Scoring overlaid in white, showing the percentage of transfected cells positive for Smchd1-GFP foci; n = 1; >85 nuclei scored.

(B) Representative nuclei following GFP IF performed in immortalized female *Smchd1*^{GFP/GFP} MEFs and primary female *Smchd1*^{GFP/GFP} NSCs following transduction, with hairpins targeting *HnrnpU*, *Lrif1*, or a non-silencing control (shNons) (n = 3). Scoring replicates shown overlaid in white, as percentages of cells with focal Smchd1-GFP enrichment following knock down ± SEMs. Scale bar represents 5 μm.

(C) Representative images from Xist RNA FISH performed in immortalized female *Smchd1*^{GFP/GFP} MEFs and primary female *Smchd1*^{GFP/GFP} NSCs following transduction, with hairpins targeting *HnrnpU* or a non-silencing control (shNons). Xist (magenta) and DAPI (gray). Representative data from n = 2; >100 nuclei scored. Percentages are mean cells that display focal Xist enrichment. Xist is still present upon *HnrnpU* knockdown, but it is

dispersed throughout the nucleus, as has been previously reported (Hasegawa et al., 2010). Scale bar represents 5 μm.

(D) Immunoprecipitation of Smchd1-GFP from *Smchd1*^{GFP/GFP} female MEFs using an antibody against GFP, and immunoprecipitation of HnrnpU using an antibody against HnrnpU, followed by western blot for Smchd1 and HnrnpU (representative of n = 3).

See also Figure S1 and Videos S1 and S2.

CTCF-GFP, which has previously been shown to directly interact with RNA molecules by PAR-CLIP (Saldaña-Meyer et al., 2014) (Figure S2). We performed a GFP immunoprecipitation in 10⁹ UV-crosslinked female *Smchd1*^{GFP/GFP} NSCs, alongside 10⁹ female *Smchd1*^{GFP/GFP} NSCs that were not irradiated with UV light, and an equal number of female *Smchd1*^{+/+} NSCs (n = 2, each in technical duplicate). We used NSCs because their growth habits make it more feasible to harvest the large numbers of cells required to perform PAR-CLIP when compared with MEFs. Upon immunoprecipitation of Smchd1-GFP, there was a discernible radioactive smear that was reduced or not present in no-crosslink or wild-type controls (Figure 2A). We excised a band corresponding to Smchd1-GFP in the PAR-CLIP gel, along with the corresponding regions in the negative controls, and purified the associated ³²P-labeled RNA for library preparation.

PAR-CLIP reads were distributed across the mouse genome (Figure 2B). PARalyzer was used to identify candidate Smchd1-GFP interacting RNAs in PAR-CLIP reads. PARalyzer uses PAR-CLIP transitions and transcript enrichment to estimate binding sites in genes (Corcoran et al., 2011). A total of 4,762 potential Smchd1 binding sites were identified in the PAR-CLIP tags. However, following normalization and background subtraction, no PARalyzer candidates were specific to Smchd1-GFP over either the no-crosslink or wild-type controls (Figures 2C, 2D, and S2). To ensure that we were not disregarding RNAs that potentially interact with Smchd1 with low frequency or affinity, we selected the strongest PAR-CLIP candidates to validate

by UV-RIP (RNA immunoprecipitation)-RT-qPCR. We could not detect enrichment of PAR-CLIP candidates *Malat1*, *Gm20388*, or *Xist* relative to housekeeping RNAs or bead-only controls following Smchd1-GFP immunoprecipitation (Figure S2).

We additionally analyzed the repetitive fraction using the HOMER analyseRepeats function and found that only tRNAs were enriched 5-fold over the no-crosslink controls and 2-fold over the wild-type controls (Heinz et al., 2010) (Figure S2). However, interrogation of individual tRNAs in Seqmonk found none that were specifically enriched over either negative control. No other repeat classes analyzed were enriched >2-fold over both negative controls, suggesting that most repetitive RNAs are not specifically enriched in the PAR-CLIP tags (Figure S2). These analyses suggest that Smchd1 does not directly bind endogenous RNA in female NSCs.

Smchd1 Does Not Directly Interact with Xist

As the Xist dependent localization of Smchd1 was observed in MEFs, we wanted to confirm that the inability to detect a direct interaction was not due to potential cell type-specific differences. To address this, we performed GFP UV-RIP alongside HnrnpU UV-RIP in immortalized female *Smchd1*^{GFP/GFP} MEFs. We found that Xist is enriched following HnrnpU IP but is not enriched upon Smchd1-GFP IP (Figure 2E), ruling out cell type-specific differences as the explanation for previous results.

Smchd1 was identified as a candidate Xist interactor using an RNA pull-down followed by a mass spectrometry (MS)

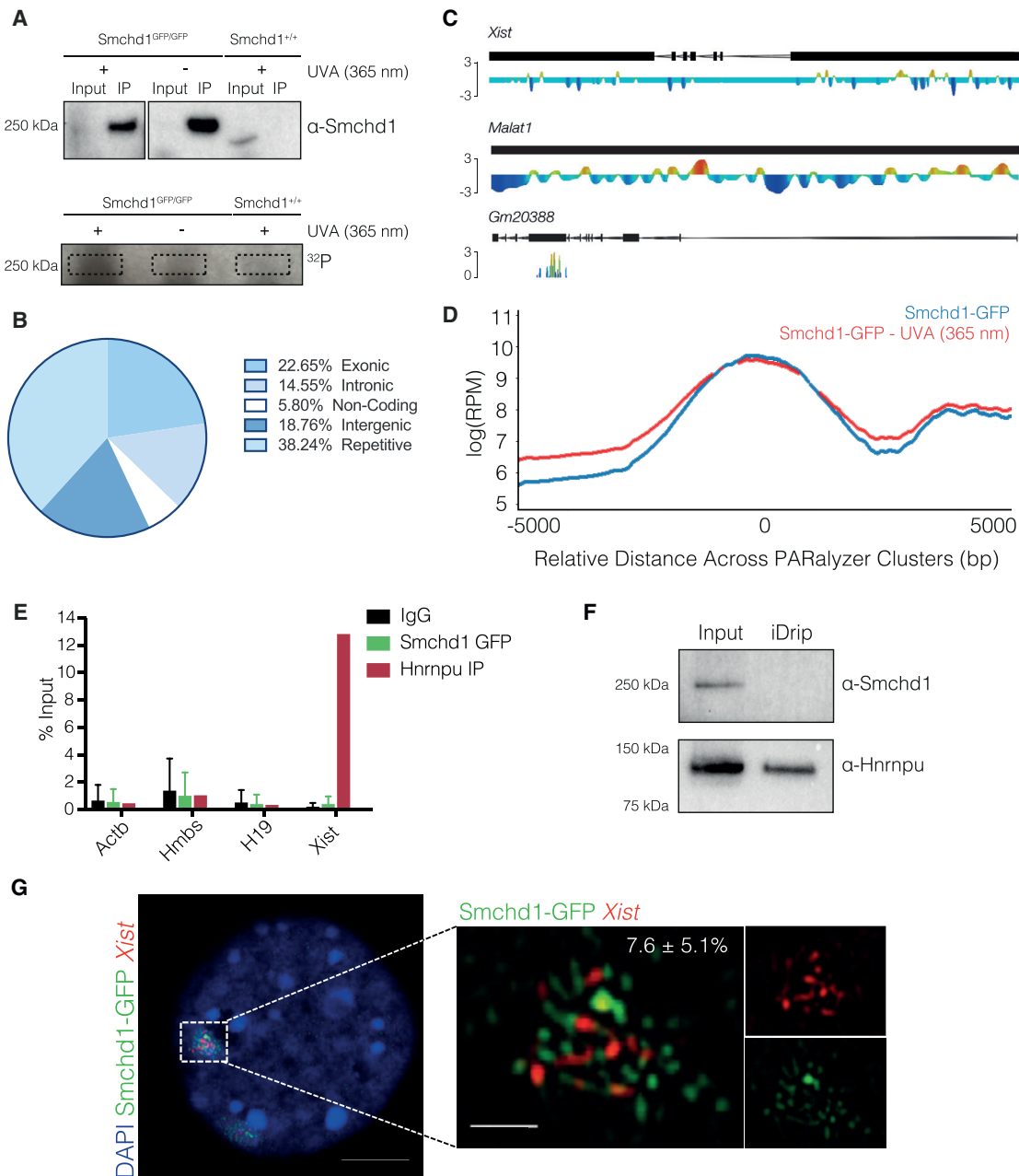


Figure 2. Smchd1 Does Not Directly or Specifically Bind to RNA In Vivo or In Vitro

(A) Western blot for Smchd1 (top) and PAR-CLIP autoradiograph following immunoprecipitation with GFP-Trap beads in *Smchd1*^{GFP/GFP} and *Smchd1*^{+/+} cells, either irradiated with UVA at 365 nm (+) or not (–).
 (B) Distribution of PAR-CLIP tags from *Smchd1*^{GFP/GFP} NSCs.
 (C) Genome browser view showing normalized Smchd1-GFP PAR-CLIP reads recovered after sequencing, subtracted for reads recovered from no-crosslink control PAR-CLIP, over the *Xist*, *Malat1*, and *Gm20388* loci. Aggregate data from n = 4. Scale bar is in reads per kilobase million (RPKM).
 (D) Coverage in log(CPM) (counts per min) of the PAR-CLIP reads centered over clusters called using PARalyzer ± 5,000 bp. Reads from *Smchd1*^{GFP/GFP} sample are represented in blue, and reads from the no-crosslink control are represented in blue.
 (E) GFP and HnrnpU UV-RIP followed by RT-qPCR for housekeeping genes and *Xist* using two different primer pairs within *Xist* in female *Smchd1*^{GFP/GFP} MEFs; n = 2.
 (F) Immunoblot for Smchd1 and HnrnpU following *Xist* enrichment by iDIP in female *Smchd1*^{GFP/GFP} NSCs. Representative data from n = 3.
 (G) High-resolution confocal imaging followed by Airyscan processing of immunofluorescent for GFP and RNA FISH for *Xist* performed in immortalized female *Smchd1*^{GFP/GFP} MEFs. Representative data from n = 2; 15 nuclei scored in 3 dimensions. Percentage of overlap = 7.6% ± 5.1%; Pearson's correlation, *R* = –0.27. See also Figure S2.

approach, although it was not validated in this publication (Minajigi et al., 2015). Therefore, we used the same technique, identification of direct RNA interacting proteins (iDRIP), which is a reciprocal approach to RIP, to test for Smchd1 enrichment following the isolation of *Xist*. Upon UV irradiation of female NSCs, we enriched for *Xist* using biotinylated antisense oligonucleotides and purified cross-linked proteins, then examined Smchd1 and HnrnpU enrichment by performing a western blot. Following the specific enrichment of *Xist* (Figure S2), HnrnpU was detected, but Smchd1 was not, which is consistent with no direct interaction between Smchd1 and *Xist* (Figure 2F).

Finally, we performed RNA FISH and immunofluorescence for *Xist* and GFP, respectively, in immortalized female *Smchd1^{GFP/GFP}* MEFs, followed by high-resolution confocal microscopy using an Airyscan detector (Zeiss). The use of the Airyscan detector increases the resolution of conventional confocal microscopy by 1.7 times, and while it does not allow for the detection of single molecules, it does enable the visualization of domains of focal enrichment in a nuclear compartment (Sivaguru et al., 2018). We found that Smchd1 and *Xist* occupy discrete territories on the Xi (percentage of overlap = $7.6\% \pm 5.1\%$, Pearson's correlation, $R = -0.27$), in support of Smchd1 and *Xist* not interacting directly on the Xi (Figure 2G).

The Affinity of Smchd1 for RNA Oligonucleotides Is Not Sequence-Specific

Although we found that Smchd1 does not bind to endogenous RNA in cells, we have previously shown that recombinant protein corresponding to the hinge domain of Smchd1 has the capacity to bind synthetic RNA oligonucleotides *in vitro* with micromolar affinity (Chen et al., 2015). We were therefore interested in investigating the nature of these interactions *in vitro*. We postulated that these interactions may arise from the highly basic composition of the recombinant hinge domain protein and could reflect the affinity of Smchd1 for DNA. Therefore, we tested whether the recombinant hinge domain of Smchd1 showed any sequence specificity toward synthetic RNA oligonucleotides. Again, we focused on *Xist*, it being the strongest candidate for a functional interaction in cells.

We performed RNA electrophoretic mobility shift assays (EMSAs) using recombinant protein corresponding to the residues that make up the hinge domain of Smchd1 and flanking coiled-coil regions (amino acid [aa] 1652–1965) and RNA oligonucleotides using the sequence of the A-repeat (RepA) region in *Xist* (Figure S2). A-repeat is a repetitive sequence within *Xist*, which forms a characteristic double hairpin-loop structure, and directly interacts with several effector proteins that are important for the establishment of silencing on the Xi. We also performed EMSAs with a mutant A-repeat RNA oligonucleotide, which is predicted to abrogate secondary structure, plus an antisense A-repeat oligonucleotide and a poly-deoxycytidylic (dC) oligonucleotide (Zhao et al., 2008). We observed that incubation with recombinant Smchd1 hinge domain protein resulted in a shift of the A-repeat RNA sequence. However, we observed a similar shift in the mutant A-repeat, antisense A-repeat, and poly-dC RNA sequences, using the same concentration of recombinant hinge domain protein (Figure S2). These data suggest that *in vitro* Smchd1 does not discern

between RNA sequences. This is consistent with non-specific binding *in vitro*.

To assay the sequence specificity of the recombinant hinge domain protein for RNAs directly, we performed competitive EMSAs using 50 nM labeled A-repeat oligonucleotides, 2.5 μ M recombinant Smchd1 hinge domain protein, and increasing concentrations of either unlabeled A-repeat RNA oligonucleotides or unlabeled poly-deoxyuridylic acid (dU). We started to observe competition between the labeled and unlabeled A-repeat RNA using a 10-fold molar excess of unlabeled: labeled probe, with complete competition at a 1,000-fold excess of unlabeled probe (Figure S2). We observed the same pattern following competition of labeled A-repeat RNA with unlabeled poly-dU of the same length (Figure S2). These data are consistent with the hinge domain of Smchd1 binding to RNA oligonucleotides *in vitro* with no sequence specificity. Our biochemical and genomic data suggest that the recombinant hinge domain of Smchd1 has a non-sequence-specific affinity for RNA *in vitro*. However, the capacity of recombinant hinge domain to bind RNA oligonucleotides *in vitro* does not confer functional binding of full-length Smchd1 to endogenous RNA in cells with any sequence specificity.

Smchd1 Localization to the Xi Is Dependent on HnrnpK

Because Smchd1 localization is dependent on *Xist*, we decided to test whether Smchd1 may interact with a characterized protein interactor of *Xist*. We analyzed Smchd1-GFP localization after depletion of epigenetic modifiers that had been identified independently in several studies as direct binding partners of *Xist*: HnrnpK, lamin B receptor (Lbr), Sin 3A associated protein 18 (Sap18), Smart/Hdac associated repressor protein (Sharp), and WT1 associated protein (Wtap) (McHugh et al., 2015; Minajigi et al., 2015; Moindrot et al., 2015; Monfort et al., 2015; Pintacuda et al., 2017). We aimed to target each protein with at least two hairpins that reduced target expression to <30% of endogenous levels. We were unable to measure expression levels for two hairpins targeting *Sharp*, because transduction with these hairpins resulted in a high level of cell death. Only one hairpin against *HnrnpK* and *Sap18* reduced target expression to <30% in each case, and therefore these genes were screened with only a single hairpin (Figure S3). Nevertheless, we found that knock down of *HnrnpK* resulted in the loss of Smchd1-GFP Xi localization in 84% of immortalized *Smchd1^{GFP/GFP}* MEFs (Figure 3A).

HnrnpK has been shown to directly interact with *Xist* but, unlike HnrnpU, it is not involved in tethering *Xist* to the Xi (Pintacuda et al., 2017). We therefore investigated whether HnrnpK and Smchd1 directly interact in female cells. We performed GFP and HnrnpK immunofluorescence in female immortalized *Smchd1^{GFP/GFP}* MEFs to determine whether HnrnpK co-localizes with Smchd1-GFP foci over the Xi territory. HnrnpK is dispersed throughout the nucleus and notably is not detectable over DAPI-dense, constitutive heterochromatin territories (Figure 3B). While it does not show focal enrichment over the territory of the Xi relative to the rest of the nucleus, HnrnpK is still present over regions of the Xi.

Analysis of confocal images with Airyscan processing show that Smchd1-GFP and HnrnpK do not overlap over the Xi in three

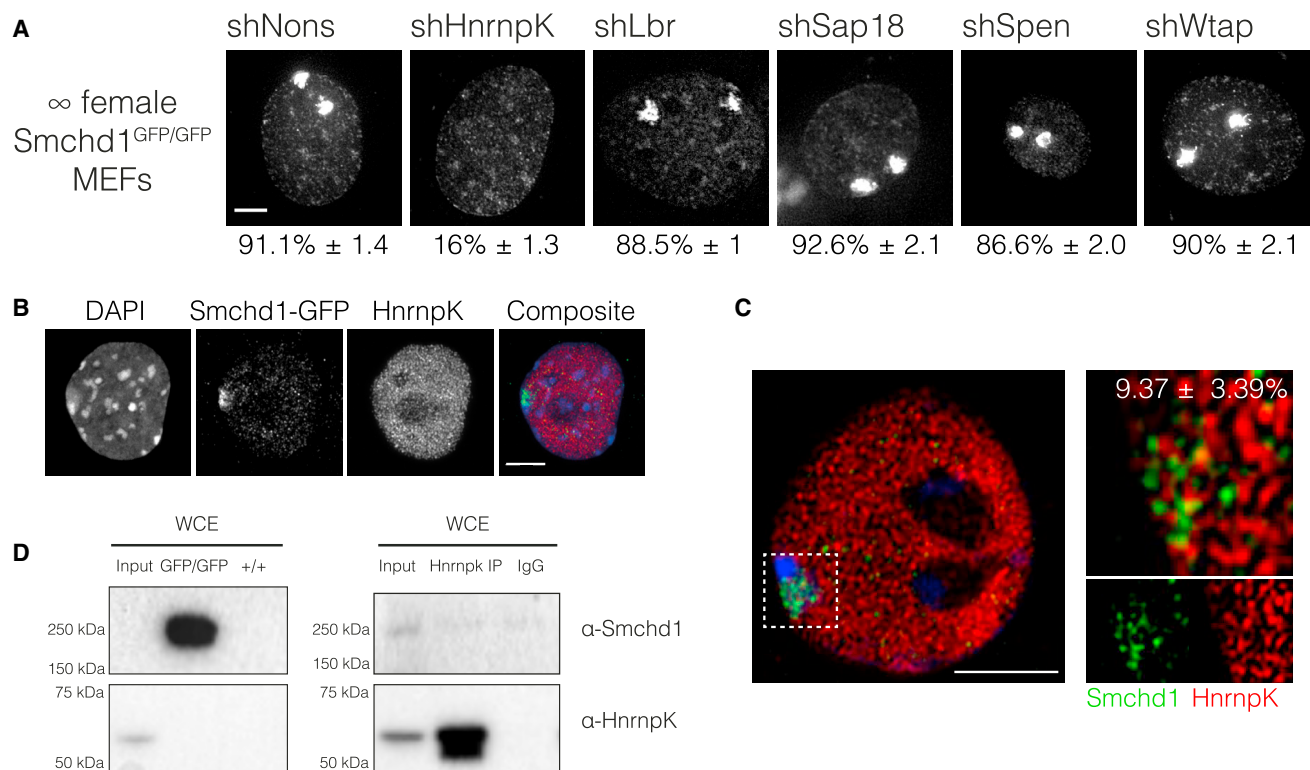


Figure 3. Smchd1 Localization to the Xi Is Dependent on HnrnpK

(A) Fluorescent imaging of native GFP in immortalized female *Smchd1*^{GFP/GFP} MEFs transduced with a non-silencing control, or hairpins targeting *HnrnpK*, *Lbr*, *Sap18*, *Spen*, or *Wtap*. Scale bar shown on non-silencing control image represents 5 μ m. Percentage of nuclei positive for Smchd1-GFP foci shown below each image. Representative data from $n = 2$; means \pm SDs displayed; >100 nuclei scored.

(B) IF for GFP and HnrnpK performed in immortalized female *Smchd1*^{GFP/GFP} MEFs. Representative data from $n = 2$.

(C) High-resolution confocal imaging followed by Airyscan processing of IF for GFP and HnrnpK performed in immortalized female *Smchd1*^{GFP/GFP} MEFs. Representative data from 10 observations, scored in 3 dimensions. Percentage of overlap = 9.37% \pm 3.39%; Pearson's correlation, $R = -0.27 \pm 0.06$. Scale bar represents 5 μ m on the image of the nucleus and 1 μ m on the magnification of the Xi.

(D) Immunoprecipitation of Smchd1-GFP using GFP-Trap beads (top), and immunoprecipitation of HnrnpK using an antibody against HnrnpK (bottom), in whole-cell extract (WCE) from immortalized female *Smchd1*^{GFP/GFP} MEFs, followed by western blot for Smchd1 and HnrnpK. Representative data from $n = 2$. See also Figure S3.

dimensions, making it unlikely that Smchd1 and HnrnpK could interact on the Xi (9.37% \pm 3.39%; Figure 3C). We performed a native IP for Smchd1-GFP and HnrnpK in whole-cell extract from female immortalized *Smchd1*^{GFP/GFP} MEFs. We were unable to detect HnrnpK enrichment following GFP-IP in the whole-cell extract, nor could we detect Smchd1 enrichment following HnrnpK-IP, suggesting that the two proteins do not directly interact in cell lysate (Figure 3D). Similar to HnrnpU knockdown, HnrnpK knockdown also does not alter Smchd1 protein or RNA expression levels (Figure S3). These data led us to explore whether Smchd1 instead depends on factors downstream of HnrnpK.

Smchd1 Recruitment to the Xi Is Dependent on the B-Repeat of *Xist*

A recent study has shown that HnrnpK recruitment to Xi is mediated by the *Xist* B/C-repeat region. HnrnpK in turn recruits the Pcgf3/5-PRC1 complex to trigger polycomb enrichment on the Xi (Almeida et al., 2017; Pintacuda et al., 2017). We therefore analyzed Smchd1 recruitment using an XX

ESC line, B2, which has a doxycycline-inducible *Xist* allele, alongside a line harboring a deletion of the *Xist* B/C-repeat region (B2 Δ B-repeat) and in a line carrying a deletion of the *Xist* A-repeat (B2 Δ A-repeat) (Figure 4A), which is a critical element required for *Xist* silencing but not for HnrnpK and polycomb recruitment (Almeida et al., 2017; Monfort et al., 2015; Wutz et al., 2002). We analyzed Smchd1 localization to the Xi using immunofluorescence (IF) after 9 days of differentiation, a time point at which Smchd1 is recruited in the majority of cells in wild-type differentiating XX ESC cultures (Gendrel et al., 2012). As illustrated in Figure 4B, Smchd1 recruitment was clearly detectable in wild-type B2 and B2 Δ A-repeat cells, but it was completely absent in B2 Δ B-repeat cells. We confirmed *Xist* transgene expression in the cell lines by RNA FISH and by co-staining for the Xi-specific marker Ciz1 (Ridings-Figueroa et al., 2017) and PRC2-mediated H3K27me3 (Figures 4C and 4D). In B2 and B2 Δ A-repeat cells, Ciz1 and H3K27me3 signals co-localize on the Xi. As expected, in B2 Δ B-repeat cultures, we observed *Xist* and Xi-associated Ciz1 but not H3K27me3. These findings indicate that the

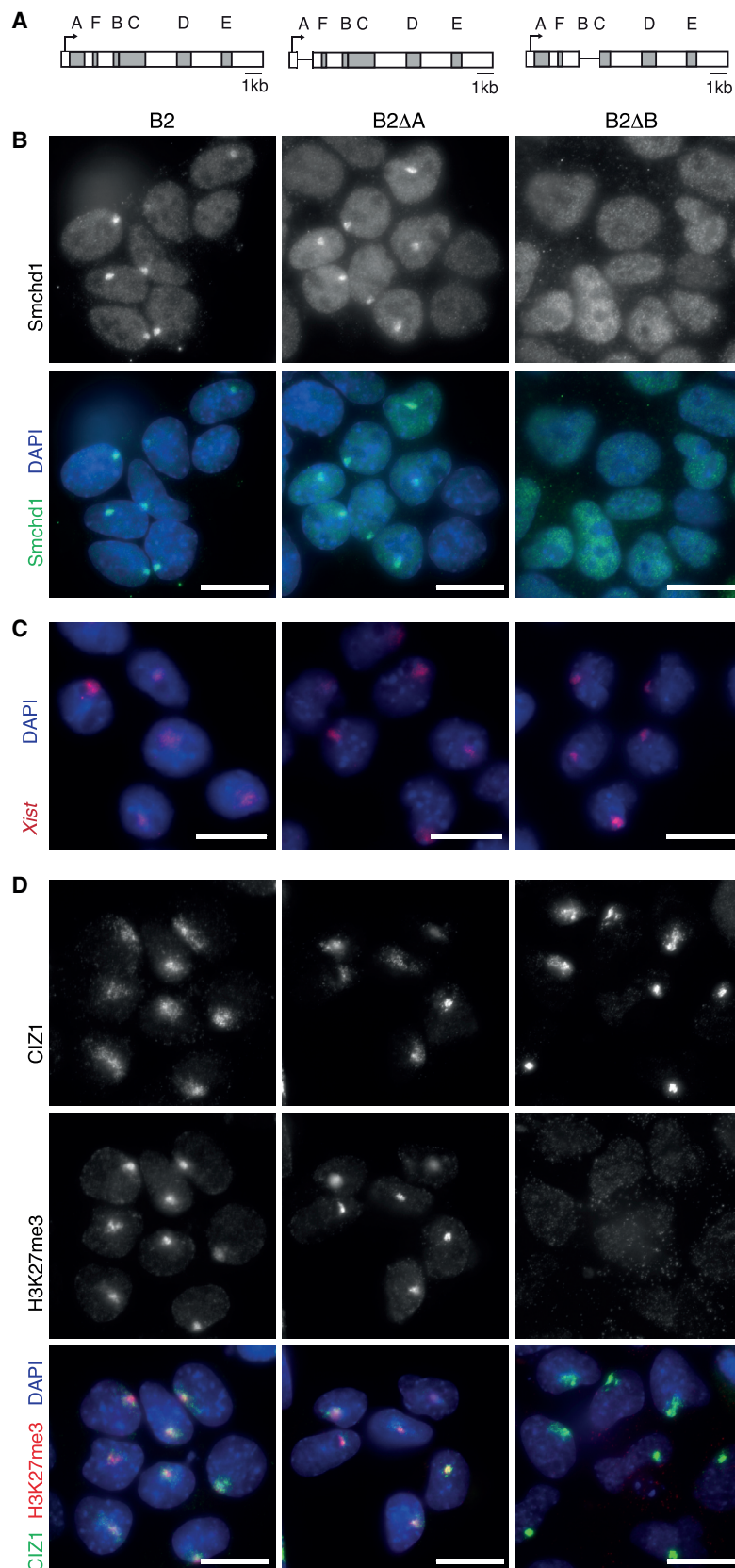


Figure 4. Smchd1 Localization to the Xi Is Dependent on the B-Repeat Region of *Xist* during Female ESC Differentiation

(A) Schematic of the wild-type doxycycline-inducible *Xist* transgene integrated on the X chromosome in XX female ESCs, and the A-repeat deleted (ΔA) and B-repeat deleted (ΔB) equivalent transgenes.

(B) IF for Smchd1 (green) with DNA counterstained with DAPI (blue) at 9 days of *Xist* induction and ESC differentiation. Left, cells containing the wild-type *Xist* transgene (B2); middle, A-repeat deleted *Xist* transgene (B2 ΔA); and right, B-repeat deleted *Xist* transgene (B2 ΔB). Scale bar indicates 20 μm . Representative data from $n = 3$.

(C) *Xist* RNA FISH (red) and DAPI (blue) in cells as for (B). Scale bar indicates 20 μm .

(D) IF for Ciz1 (green) and H3K27me3 (red), with DNA stained with DAPI (blue), in cells as for (B). Scale bar indicates 20 μm . Representative data from $n = 3$.

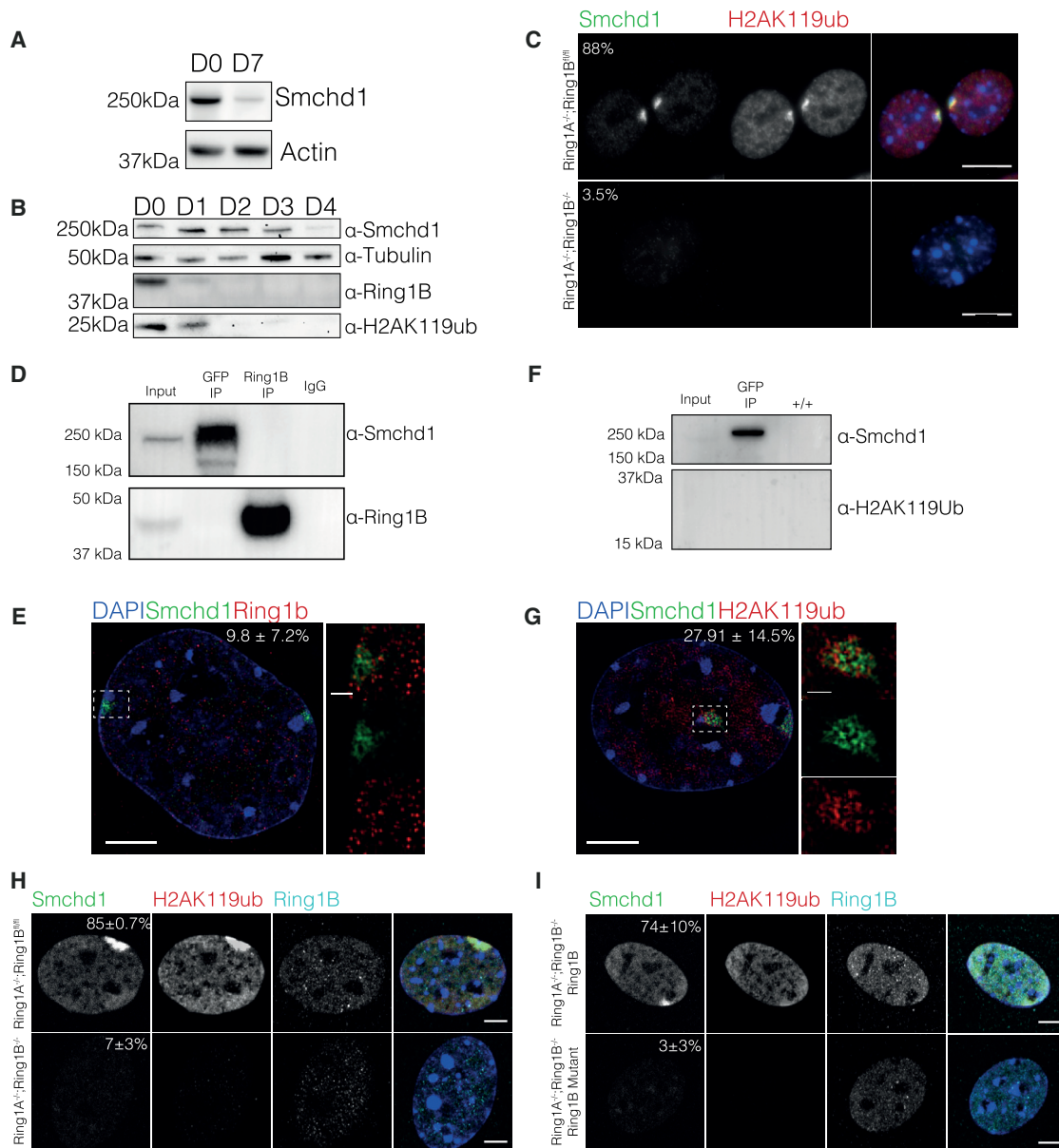


Figure 5. Smchd1 Localization to the Xi Is Dependent on Polycomb Repressive Complex 1

(A) Western blot for Smchd1 and actin in WCE from primary female *Ring1A*^{-/-}; *Ring1B*^{fl/fl} and *Ring1A*^{-/-}; *Ring1B*^{del/del} MEFs 7 days following induction of Cre-ERT2 to delete *Ring1B*. Representative data from n = 2.

(B) Western blot for Smchd1, tubulin, Ring1B, and H2AK119ub in WCE from primary female *Ring1A*^{-/-}; *Ring1B*^{fl/fl} at 0–4 days following induction of Cre-ERT2 to delete *Ring1B*. Representative data from n = 3.

(C) IF for Smchd1, Ring1B, and H2AK119ub in female *Ring1A*^{-/-}; *Ring1B*^{fl/fl} and *Ring1A*^{-/-}; *Ring1B*^{del/del} MEFs at day 7 post-deletion. Scale bar represents 5 μ m. Percentage in the top left of the Smchd1 IF image indicates the proportion of cells that display distribution of Smchd1-GFP represented in each panel. Representative data from n = 2; mean displayed; >50 nuclei scored.

(D) Immunoprecipitation of Smchd1-GFP using an antibody against GFP and immunoprecipitation of Ring1B in WCE from immortalized female *Smchd1*^{GFP/GFP} MEFs, followed by western blot for Smchd1 and Ring1B. Representative data from n = 2.

(E) 3D-SIM imaging of IF for GFP (green) and Ring1B (red) performed in immortalized female *Smchd1*^{GFP/GFP} MEFs. Representative image from n = 2; 40 measurements. Percentage of overlap = 9.9% \pm 2.5%. Scale bar represents 5 μ m on the image of the nucleus and 1 μ m on the magnification of the Xi.

(F) Immunoprecipitation of Smchd1-GFP using an antibody against Smchd1-GFP and immunoprecipitation of H2AK119ub in WCE from immortalized female *Smchd1*^{GFP/GFP} MEFs, followed by western blot for Smchd1 and H2AK119ub. Representative data from n = 2.

(G) 3D-SIM imaging of IF for GFP (green) and H2AK119ub (red) performed in immortalized female *Smchd1*^{GFP/GFP} MEFs. Representative image from n = 2; 20 measurements. Percentage of overlap = 29% \pm 7.4%. Scale bar represents 5 μ m on the image of the nucleus and 1 μ m on the magnification of the Xi.

(legend continued on next page)

Xist B-repeat region is required both for Smchd1 and polycomb enrichment on the Xi.

Smchd1 Localization to the Xi and Global Stability Are Dependent on PRC1

Given that HnmpK recruits non-canonical PRC1, which in turn recruits PRC2 and canonical PRC1 (Almeida et al., 2017; Pintacuda et al., 2017), we next sought to test whether Smchd1 recruitment to the Xi was polycomb dependent. Notably, HnmpK also has a role in maintaining polycomb enrichment during the maintenance of *Xist*-mediated gene silencing; knock down of HnmpK results in a reduction of focal H2AK119ub and H3K27me3 enrichment over areas of focal *Xist* enrichment in e36 cells that overexpress an *Xist* transgene on chromosome 10 (Pintacuda et al., 2017). We performed IF for Smchd1 in female MEFs in which we genetically deleted *Ezh2*, the primary enzyme in PRC2 that catalyzes H3K27me3 (Cao et al., 2002). *Ezh2* deletion left Smchd1 focal enrichment unperturbed (Figure S4). Next, we sought to test the dependence of Smchd1 localization to the Xi on *Ring1A* (also known as *Ring1*) and *Ring1B* (also known as *Rnf2*), the PRC1 components that catalyze H2AK119ub. Unlike any of the other factors we tested, Smchd1 protein stability, but not expression of *Smchd1* mRNA, was dependent on *Ring1B* in the context of *Ring1A* null cells (Figures 5A, 5B, and S4). We measured Smchd1 protein levels daily alongside *Ring1B* and H2AK119ub for 4 days following *Ring1B* deletion, and then again at day 7 post-deletion. Smchd1 levels remained stable for 3 days, but declined after that (Figures 5A and 5B). While *Ring1B* can no longer be detected 1 day after *Ring1B* deletion, we could detect H2AK119ub signal until 2 days post-*Ring1B* deletion. Therefore, we performed IF for Smchd1, *Ring1B*, and H2AK119ub 3 and 7 days post-*Ring1B* deletion. Deletion of *Ring1A* alone did not result in a loss of Smchd1 from the Xi territory (Figure 5C). In contrast, removal of both *Ring1A* and *Ring1B* resulted in the loss of Smchd1 focal enrichment in 81% and 96.5% of female nuclei at 3 and 7 days post-*Ring1B* deletion, respectively (Figures 5C and S4). Given the dependency of Smchd1 on PRC1, we tested whether Smchd1 co-localizes or co-immunoprecipitates with *Ring1B*. Native Smchd1-GFP did not co-immunoprecipitate with *Ring1B* in the whole-cell extract from female Smchd1-GFP MEFs (Figure 5D), nor did Smchd1 overlap with *Ring1B* ($9.9\% \pm 2.5\%$) over the Xi territory in our analysis of three-dimensional-structured illumination microscopy (3D-SIM) images of female MEFs following IF (Figure 5E). Together, these data suggest that Smchd1 localization to the Xi in interphase is dependent on PRC1.

Smchd1 Localization to the Xi and Global Stability Are Dependent on H2AK119ub

We next sought to test whether it was the H2AK119ub mark catalysed by PRC1 that recruits Smchd1 to the Xi and is required for Smchd1 stability. In our previous IF experiment, while we could

not detect H2AK119ub in the majority of *Ring1A*^{-/-}; *Ring1B*^{del/del} nuclei (12%), we identified a subset of nuclei that retained H2AK119ub in the absence of *Ring1B*. Notably, these cells also displayed focal Smchd1 enrichment (Figure S4), suggesting that Smchd1 depends on H2AK119ub. While we could not immunoprecipitate Smchd1 with H2AK119ub, we found a higher co-localization with H2AK119ub ($29\% \pm 7.4\%$; Figures 5F and 5G) than with any of the other factors previously tested. These data suggest that Smchd1 may depend on H2AK119ub for localization to the Xi. To formally test this possibility, we overexpressed wild-type *Ring1B*, or a mutant form of *Ring1B* that cannot catalyze H2AK119ub (Bentley et al., 2011; Buchwald et al., 2006; Elderkin et al., 2007), in *Ring1A*^{-/-}; *Ring1B*^{del/del} cells. We found that only wild-type *Ring1B* was able to restore H2AK119ub, reinstate Smchd1 localization to the Xi, and rescue the stability of Smchd1 (Figures 5H, 5I, and S4). These data suggest that the Xi localization of Smchd1 is dependent on H2AK119ub-marked chromatin and that PRC1-mediated H2AK119ub is globally required for Smchd1 stability.

DISCUSSION

In recent years, growing evidence has suggested that Smchd1 may directly interact with RNA. SMCHD1 is dependent on *XIST* RNA for its localization to the Xi, and SMCHD1 is recruited to some autosomal loci upon induction of an autosomal *XIST* transgene (Kelsey et al., 2015; Nozawa et al., 2013). More recently, Smchd1 was identified as a candidate interaction partner of *Xist* in MEFs by iDRIP, and we showed that recombinant protein corresponding to the hinge domain of Smchd1 has the capacity to bind synthetic RNA oligonucleotides *in vitro* (Chen et al., 2015; Minajigi et al., 2015). We have presented the first investigation into Smchd1 as an RNA binding protein and have found using multiple genomic and biochemical approaches that Smchd1 does not directly interact with *Xist*, nor with other endogenous RNA species genome-wide in female NSCs with any specificity. This implies that direct interactions between Smchd1 and RNA molecules are not likely to be important for the chromosomal localization of Smchd1. However, because these experiments were performed in committed cells, generally in interphase, we cannot rule out that Smchd1 interacts transiently with RNA during mitosis or, potentially, during a defined developmental window for its initial recruitment to the chromatin.

While we could not detect interactions between endogenous full-length Smchd1 and endogenous RNA molecules using PAR-CLIP, recombinant Smchd1 hinge domain does have the capacity to bind to both synthetic RNA and DNA oligonucleotides *in vitro* (Chen et al., 2015). In the present study, we have shown that the binding of Smchd1 to RNA oligonucleotides is not sequence specific. When considering this in the context of our current PAR-CLIP data and our previously reported chromatin immunoprecipitation sequencing (ChIP-seq) data (Chen

(H and I) IF for Smchd1, *Ring1B*, and H2AK119ub in cells with the same genetics as in (C) is shown in (H), overexpressing either wild-type *Ring1B* or catalytically inactive *Ring1B* (I), analyzed at day 4 post-deletion and rescue. Scale bar represents 5 μ m. Percentage in the top left of the Smchd1 IF image indicates the proportion of cells that display distribution of Smchd1 represented in each panel. Representative data from $n = 2$; mean displayed; >75 nuclei scored. See also Figure S4.

et al., 2015; Jansz et al., 2018), we postulate that the non-sequence specific binding *in vitro* may reflect the capacity of the protein to bind DNA *in vivo*. Previous work from our group has characterized a mutant form of SMCHD1 that has been found to underlie facioscapulohumeral muscular dystrophy type 2 (FSHD2) and found that the mutation in the hinge domain reduces the capacity of the recombinant protein to bind to nucleic acids (Chen et al., 2015). Taken together with our current work, these data suggest that DNA rather than RNA binding is of important functional relevance to Smchd1.

Screening for downstream RNA binding proteins allowed us to place Smchd1 in the *Xist*-HnnpK-PRC1 silencing pathway. The Xi localization of Smchd1 is dependent on PRC1 but notably not on Ezh2-PRC2, which is consistent with PRC2 acting downstream of PRC1 on the Xi (Almeida et al., 2017; Schoeftner et al., 2006). Moreover, we found that Smchd1 specifically depends on the PRC1-dependent mark H2AK119ub both for localization to the Xi and protein stability. While we could not detect a direct interaction between H2AK119ub and Smchd1 in cell lysate, we did detect overlap of H2AK119ub and Smchd1 domains on the Xi. Given that Smchd1 is not predicted to harbor a conventional ubiquitin-binding domain, we propose that either there is an as-yet unidentified adaptor protein that links H2AK119ub and Smchd1 or the presence of H2AK119ub creates a local chromatin environment or separate phase that can be permeabilized by Smchd1. For the Xi, our LNA data suggest that *Xist* may also be required for phase permeability to Smchd1. In the absence of H2AK119ub, the local environment is impermeable to Smchd1. A subsequent reduction in Smchd1 protein levels suggests that continued association with the chromatin is important for protein stability. The stabilization of Smchd1 may occur through a PRC1-mediated chromatin environment that is perturbed in conditions needed to lyse cells. Another possibility is that direct association with the chromatin itself stabilizes Smchd1 protein, which is predicted to contain a large central flexible region.

Although the majority of our experiments were performed in the maintenance stage of XCI, we also addressed how Smchd1 is recruited during the establishment of XCI using a female ESC differentiation model. In this case, we were able to show that Smchd1 recruitment is dependent on the B-repeat of *Xist*, as expected given the dependence on the HnnpK-PRC1 pathway. These data suggest that the initial targeting of Smchd1 to the Xi happens via the same pathway as the maintenance of Smchd1 on the Xi.

In conclusion, we have provided genomic and biochemical evidence to suggest that Smchd1 does not directly interact with endogenous RNA in cells. This is of relevance due to a growing assumption that Smchd1 is a direct interactor of *Xist*, based on its dependence on *XIST* for its Xi localization (Nozawa et al., 2013) and its recent identification as a candidate *Xist* interactor by iDRIP (Minajigi et al., 2015). We provide further support for published data in immortalized MEFs and in primary NSCs, which suggests that the interaction between *Lrlf1* and Smchd1 on the Xi is not important for the focal enrichment of Smchd1 over the Xi territory in mouse. We instead find that Smchd1 localization to the Xi is dependent on the HnnpK-PRC1 pathway. We also find that global Smchd1 stability relies

on PRC1-mediated H2AK119ub. Our data raise the exciting possibility that Smchd1 and PRC1 functionally interact to elicit gene silencing on the Xi and potentially genome-wide. Relevant to this, Smchd1 is highly enriched at the four *Hox* clusters in mice, at which PRC1 is important in forming compact domains, and at other polycomb-enriched loci genome-wide (Chen et al., 2015; Endoh et al., 2012; Eskeland et al., 2010; Jansz et al., 2018; Lau et al., 2017). These Smchd1 targets are not H3K9 methylation targets; therefore, we propose two mechanisms of Smchd1 recruitment: one involving H3K9 methylation, *Hp1* γ , and *Lrlf1*, and the other relevant to the Xi and the *Hox* genes at least, requiring PRC1-mediated H2AK119ub.

STAR★METHODS

Detailed methods are provided in the online version of this paper and include the following:

- KEY RESOURCES TABLE
- CONTACT FOR REAGENT AND RESOURCE SHARING
- EXPERIMENTAL MODEL AND SUBJECT DETAILS
 - Animal husbandry and ethics
 - *Smchd1*^{GFP/GFP} Mice
 - *Smchd1*^{GFP/GFP}; *Ezh2*^{fl/fl} Mice and MEFs
 - *Ring1A*^{-/-}; *Ring1B*^{fl/fl}, *Rosa26::CreERT2* Mice and MEFs
 - Derivation and culture of Mouse Embryonic Fibroblasts (MEFs)
 - Derivation of Neural Stem Cells (NSCs)
 - *Xist* mutant ES cells
- METHOD DETAILS
 - Oligonucleotides and Vectors
 - Ligation
 - Transformation
 - Plasmid Preparation
 - Sequencing Plasmids
 - Retrovirus Production
 - Concentration of Retrovirus with PEG
 - Transduction of MEFs
 - Transduction of NSCs
 - RNA Extraction
 - Reverse Transcription of RNA
 - RT-qPCR
 - Live Cell Imaging
 - Immunofluorescence
 - *Xist* RNA FISH
 - GFP Immunofluorescence and *Xist* RNA FISH
 - 3D SIM
 - Preparation of Whole Cell Extract and Fractionation
 - Protein Quantification
 - Silver Stain
 - Western Blot
 - Immunoprecipitation
 - PAR-CLIP
 - RNA Immunoprecipitation (RIP)
 - Identification of Direct RNA interacting Proteins (iDRIP)
 - Recombinant Protein Expression
 - EMSAs

- **QUANTIFICATION AND STATISTICAL ANALYSIS**
 - T-Tests for Imaging and Knockdown Data
 - PAR-CLIP
 - Colocalisation Analyses
- **DATA AND SOFTWARE AVAILABILITY**

SUPPLEMENTAL INFORMATION

Supplemental Information includes four figures, one table, and two videos and can be found with this article online at <https://doi.org/10.1016/j.celrep.2018.10.044>.

ACKNOWLEDGMENTS

This work was funded by the Australian National Health and Medical Research Council grant to M.E.B. and J.M.M. (GNT1098290) and fellowship to J.M.M. (GNT1105754). N.J. was supported by an Australian Research Training Program Fellowship. M.E.B. was supported by a Bellberry-Viertel Senior Medical Research Fellowship. This work was made possible through the Victorian State Government Operational Infrastructure Support and the Australian National Health and Medical Research Council Research Institute Infrastructure Support scheme.

AUTHOR CONTRIBUTIONS

N.J. designed and performed experiments, interpreted and analyzed the data, and wrote the paper. T.N. designed and performed experiments and interpreted and analyzed the data. A.K. and P.F.H. contributed to the bioinformatic analyses of the data. S.K., K.A.B., and M.I. performed experiments. O.M., G.P., and T.A.W. designed and performed experiments. H.K. and G.F.K. designed experiments. A.H.F., N.B., and J.M.M. designed experiments and interpreted data. M.E.B. designed experiments, interpreted data, and wrote the paper. All of the authors edited the paper.

DECLARATION OF INTERESTS

The authors declare no competing interests.

Received: June 29, 2018

Revised: September 6, 2018

Accepted: October 11, 2018

Published: November 13, 2018

REFERENCES

- Almeida, M., Pintacuda, G., Masui, O., Koseki, Y., Gdula, M., Cerase, A., Brown, D., Mould, A., Innocent, C., Nakayama, M., et al. (2017). PCGF3/5-PRC1 initiates Polycomb recruitment in X chromosome inactivation. *Science* 356, 1081–1084.
- Ball, G., Demmerle, J., Kaufmann, R., Davis, I., Dobbie, I.M., and Schermelleh, L. (2015). SIMcheck: a toolbox for successful super-resolution structured illumination microscopy. *Sci. Rep.* 5, 15915.
- Bentley, M.L., Corn, J.E., Dong, K.C., Phung, Q., Cheung, T.K., and Cochran, A.G. (2011). Recognition of UbcH5c and the nucleosome by the Bmi1/Ring1b ubiquitin ligase complex. *EMBO J.* 30, 3285–3297.
- Blewitt, M.E., Gendrel, A.-V., Pang, Z., Sparrow, D.B., Whitelaw, N., Craig, J.M., Apedaile, A., Hilton, D.J., Dunwoodie, S.L., Brockdorff, N., et al. (2008). SmcHD1, containing a structural-maintenance-of-chromosomes hinge domain, has a critical role in X inactivation. *Nat. Genet.* 40, 663–669.
- Brideau, N.J., Coker, H., Gendrel, A.-V., Siebert, C.A., Bezstarosti, K., Demmers, J., Poot, R.A., Nesterova, T.B., and Brockdorff, N. (2015). Independent mechanisms target SMCHD1 to trimethylated histone H3 lysine 9-modified chromatin and the inactive X chromosome. *Mol. Cell. Biol.* 35, 4053–4068.
- Brockdorff, N. (2017). Polycomb complexes in X chromosome inactivation. *Philos. Trans. R. Soc. Lond. B Biol. Sci.* 372, 20170021.
- Brockdorff, N., Ashworth, A., Kay, G.F., McCabe, V.M., Norris, D.P., Cooper, P.J., Swift, S., and Rastan, S. (1992). The product of the mouse Xist gene is a 15 kb inactive X-specific transcript containing no conserved ORF and located in the nucleus. *Cell* 71, 515–526.
- Brown, C.J., Ballabio, A., Rupert, J.L., Lafreniere, R.G., Grompe, M., Tonlorenzi, R., and Willard, H.F. (1991). A gene from the region of the human X inactivation centre is expressed exclusively from the inactive X chromosome. *Nature* 349, 38–44.
- Buchwald, G., van der Stoep, P., Weichenrieder, O., Perrakis, A., van Lohuizen, M., and Sixma, T.K. (2006). Structure and E3-ligase activity of the Ring-Ring complex of polycomb proteins Bmi1 and Ring1b. *EMBO J.* 25, 2465–2474.
- Calés, C., Román-Trufero, M., Pavón, L., Serrano, I., Melgar, T., Endoh, M., Pérez, C., Koseki, H., and Vidal, M. (2008). Inactivation of the polycomb group protein Ring1B unveils an antiproliferative role in hematopoietic cell expansion and cooperation with tumorigenesis associated with Ink4a deletion. *Mol. Cell. Biol.* 28, 1018–1028.
- Cao, R., Wang, L., Wang, H., Xia, L., Erdjument-Bromage, H., Tempst, P., Jones, R.S., and Zhang, Y. (2002). Role of histone H3 lysine 27 methylation in Polycomb-group silencing. *Science* 298, 1039–1043.
- Chaumeil, J., Augui, S., Chow, J.C., and Heard, E. (2008). Combined immunofluorescence, RNA fluorescent in situ hybridization, and DNA fluorescent in situ hybridization to study chromatin changes, transcriptional activity, nuclear organization, and X-chromosome inactivation. *Methods Mol. Biol.* 463, 297–308.
- Chen, K., Hu, J., Moore, D.L., Liu, R., Kessans, S.A., Breslin, K., Lucet, I.S., Keniry, A., Leong, H.S., Parish, C.L., et al. (2015). Genome-wide binding and mechanistic analyses of SmcHD1-mediated epigenetic regulation. *Proc. Natl. Acad. Sci. USA* 112, E3535–E3544.
- Corcoran, D.L., Georgiev, S., Mukherjee, N., Gottwein, E., Skalsky, R.L., Keene, J.D., and Ohler, U. (2011). PARalyzer: definition of RNA binding sites from PAR-CLIP short-read sequence data. *Genome Biol.* 12, R79.
- del Mar Lorente, M., Marcos-Gutiérrez, C., Pérez, C., Schoorlemmer, J., Ramírez, A., Magin, T., and Vidal, M. (2000). Loss- and gain-of-function mutations show a polycomb group function for Ring1A in mice. *Development* 127, 5093–5100.
- Dickins, R.A., Hemann, M.T., Zilfou, J.T., Simpson, D.R., Ibarra, I., Hannon, G.J., and Lowe, S.W. (2005). Probing tumor phenotypes using stable and regulated synthetic microRNA precursors. *Nat. Genet.* 37, 1289–1295.
- Dow, L.E., Premrsirut, P.K., Zuber, J., Fellmann, C., McJunkin, K., Miething, C., Park, Y., Dickins, R.A., Hannon, G.J., and Lowe, S.W. (2012). A pipeline for the generation of shRNA transgenic mice. *Nat. Protoc.* 7, 374–393.
- Elderkin, S., Maertens, G.N., Endoh, M., Mallery, D.L., Morrice, N., Koseki, H., Peters, G., Brockdorff, N., and Hiom, K. (2007). A phosphorylated form of Mel-18 targets the Ring1B histone H2A ubiquitin ligase to chromatin. *Mol. Cell* 28, 107–120.
- Endoh, M., Endo, T.A., Endoh, T., Fujimura, Y., Ohara, O., Toyoda, T., Otte, A.P., Okano, M., Brockdorff, N., Vidal, M., and Koseki, H. (2008). Polycomb group proteins Ring1A/B are functionally linked to the core transcriptional regulatory circuitry to maintain ES cell identity. *Development* 135, 1513–1524.
- Endoh, M., Endo, T.A., Endoh, T., Isono, K., Sharif, J., Ohara, O., Toyoda, T., Ito, T., Eskeland, R., Bickmore, W.A., et al. (2012). Histone H2A mono-ubiquitination is a crucial step to mediate PRC1-dependent repression of developmental genes to maintain ES cell identity. *PLoS Genet.* 8, e1002774.
- Eskeland, R., Leeb, M., Grimes, G.R., Kress, C., Boyle, S., Sproul, D., Gilbert, N., Fan, Y., Skoultschi, A.I., Wutz, A., and Bickmore, W.A. (2010). Ring1B compacts chromatin structure and represses gene expression independent of histone ubiquitination. *Mol. Cell* 38, 452–464.
- Gdula, M.R., Nesterova, T.B., Pintacuda, G., Godwin, J., Zhan, Y., Ozadam, H., McClellan, M., Moralli, D., Krueger, F., Green, C.M., et al. (2018). The non-canonical SMC protein SmcHD1 antagonises TAD formation on the inactive X chromosome. *bioRxiv*. <https://doi.org/10.1101/342147>.

- Gendrel, A.V., Apedaile, A., Coker, H., Termanis, A., Zvetkova, I., Godwin, J., Tang, Y.A., Huntley, D., Montana, G., Taylor, S., et al. (2012). Smchd1-dependent and -independent pathways determine developmental dynamics of CpG island methylation on the inactive X chromosome. *Dev. Cell* 23, 265–279.
- Gendrel, A.-V., Tang, Y.A., Suzuki, M., Godwin, J., Nesterova, T.B., Grealis, J.M., Heard, E., and Brockdorff, N. (2013). Epigenetic functions of smchd1 repress gene clusters on the inactive X chromosome and on autosomes. *Mol. Cell. Biol.* 33, 3150–3165.
- Hafner, M., Landthaler, M., Burger, L., Khorshid, M., Hausser, J., Berninger, P., Rothballer, A., Ascano, M., Jungkamp, A.-C., Munschauer, M., et al. (2010). PAR-CLIP—a method to identify transcriptome-wide the binding sites of RNA binding proteins. *J. Vis. Exp.* (41), 2034.
- Hasegawa, Y., Brockdorff, N., Kawano, S., Tsutui, K., Tsutui, K., and Nakagawa, S. (2010). The matrix protein hnRNP U is required for chromosomal localization of Xist RNA. *Dev. Cell* 19, 469–476.
- Heinz, S., Benner, C., Spann, N., Bertolino, E., Lin, Y.C., Laslo, P., Cheng, J.X., Murre, C., Singh, H., and Glass, C.K. (2010). Simple combinations of lineage-determining transcription factors prime cis-regulatory elements required for macrophage and B cell identities. *Mol. Cell* 38, 576–589.
- Jansz, N., Keniry, A., Trussart, M., Bildsoe, H., Beck, T., Tonks, I.D., Mould, A.W., Hickey, P., Breslin, K., Iminoff, M., et al. (2018). Long-range chromatin interactions on the inactive X and at Hox clusters are regulated by the non-canonical SMC protein Smchd1. *bioRxiv*. <https://doi.org/10.1101/342212>.
- Kay, G.F., Penny, G.D., Patel, D., Ashworth, A., Brockdorff, N., and Rastan, S. (1993). Expression of Xist during mouse development suggests a role in the initiation of X chromosome inactivation. *Cell* 72, 171–182.
- Kelsey, A.D., Yang, C., Leung, D., Minks, J., Dixon-McDougall, T., Baldry, S.E.L., Bogutz, A.B., Lefebvre, L., and Brown, C.J. (2015). Impact of flanking chromosomal sequences on localization and silencing by the human non-coding RNA XIST. *Genome Biol.* 16, 208.
- Kim, D., Pertea, G., Trapnell, C., Pimentel, H., Kelley, R., and Salzberg, S.L. (2013). TopHat2: accurate alignment of transcriptomes in the presence of insertions, deletions and gene fusions. *Genome Biol.* 14, R36.
- Kinkel, S.A., Galeev, R., Flensburg, C., Keniry, A., Breslin, K., Gilan, O., Lee, S., Liu, J., Chen, K., Gearing, L.J., et al. (2015). Jarid2 regulates hematopoietic stem cell function by acting with polycomb repressive complex 2. *Blood* 125, 1890–1900.
- Kolpa, H.J., Fackelmayer, F.O., and Lawrence, J.B. (2016). SAF-a requirement in anchoring XIST RNA to chromatin varies in transformed and primary cells. *Dev. Cell* 39, 9–10.
- Larionov, A., Krause, A., and Miller, W. (2005). A standard curve based method for relative real time PCR data processing. *BMC Bioinformatics* 6, 62.
- Lau, M.S., Schwartz, M.G., Kundu, S., Savol, A.J., Wang, P.I., Marr, S.K., Grau, D.J., Schorderet, P., Sadreyev, R.I., Tabin, C.J., and Kingston, R.E. (2017). Mutation of a nucleosome compaction region disrupts Polycomb-mediated axial patterning. *Science* 355, 1081–1084.
- Leong, H.S., Chen, K., Hu, Y., Lee, S., Corbin, J., Pakusch, M., Murphy, J.M., Majewski, I.J., Smyth, G.K., Alexander, W.S., et al. (2013). Epigenetic regulator Smchd1 functions as a tumor suppressor. *Cancer Res.* 73, 1591–1599.
- Lyon, M.F. (1961). Gene action in the X-chromosome of the mouse (*Mus musculus* L.). *Nature* 190, 372–373.
- Majewski, I.J., Blewitt, M.E., de Graaf, C.A., McManus, E.J., Bahlo, M., Hilton, A.A., Hyland, C.D., Smyth, G.K., Corbin, J.E., Metcalf, D., et al. (2008). Polycomb repressive complex 2 (PRC2) restricts hematopoietic stem cell activity. *PLoS Biol.* 6, e93.
- McHugh, C.A., Chen, C.-K., Chow, A., Surka, C.F., Tran, C., McDonnell, P., Pandya-Jones, A., Blanco, M., Burghard, C., Moradian, A., et al. (2015). The Xist lncRNA interacts directly with SHARP to silence transcription through HDAC3. *Nature* 521, 232–236.
- Minajigi, A., Froberg, J., Wei, C., Sunwoo, H., Kesner, B., Colognori, D., Lessing, D., Payer, B., Boukhali, M., Haas, W., and Lee, J.T. (2015). Chromosomes. A comprehensive Xist interactome reveals cohesin repulsion and an RNA-directed chromosome conformation. *Science* 349. <https://doi.org/10.1126/science.aab2276>.
- Moindrot, B., Cerase, A., Coker, H., Masui, O., Grijzenhout, A., Pintacuda, G., Schermelleh, L., Nesterova, T.B., and Brockdorff, N. (2015). A pooled shRNA screen identifies Rbm15, Spen, and Wtap as factors required for Xist RNA-mediated silencing. *Cell Rep.* 12, 562–572.
- Monfort, A., Di Minin, G., Postlmayr, A., Freimann, R., Arieti, F., Thore, S., and Wutz, A. (2015). Identification of Spen as a crucial factor for Xist function through forward genetic screening in haploid embryonic stem cells. *Cell Rep.* 12, 554–561.
- Mould, A.W., Pang, Z., Pakusch, M., Tonks, I.D., Stark, M., Carrie, D., Mukhopadhyay, P., Seidel, A., Ellis, J.J., Deakin, J., et al. (2013). Smchd1 regulates a subset of autosomal genes subject to monoallelic expression in addition to being critical for X inactivation. *Epigenetics Chromatin* 6, 19.
- Nozawa, R.-S., Nagao, K., Igami, K.-T., Shibata, S., Shirai, N., Nozaki, N., Sado, T., Kimura, H., and Obuse, C. (2013). Human inactive X chromosome is compacted through a PRC2-independent SMCHD1-HBIX1 pathway. *Nat. Struct. Mol. Biol.* 20, 566–573.
- Penny, G.D., Kay, G.F., Sheardown, S.A., Rastan, S., and Brockdorff, N. (1996). Requirement for Xist in X chromosome inactivation. *Nature* 379, 131–137.
- Pintacuda, G., Wei, G., Roustan, C., Kirmizitas, B.A., Solcan, N., Cerase, A., Castello, A., Mohammed, S., Moindrot, B., Nesterova, T.B., et al. (2017). hnRNPK recruits PCGF3/5-PRC1 to the Xist RNA B-repeat to establish polycomb-mediated chromosomal silencing. *Mol. Cell* 68, 955–969.e10.
- Ridings-Figueroa, R., Stewart, E.R., Nesterova, T.B., Coker, H., Pintacuda, G., Godwin, J., Wilson, R., Haslam, A., Lilley, F., Ruigrok, R., et al. (2017). The nuclear matrix protein CIZ1 facilitates localization of Xist RNA to the inactive X-chromosome territory. *Genes Dev.* 31, 876–888.
- Saldaña-Meyer, R., González-Buendía, E., Guerrero, G., Narendra, V., Bonasio, R., Recillas-Targa, F., and Reinberg, D. (2014). CTCF regulates the human p53 gene through direct interaction with its natural antisense transcript, Wrap53. *Genes Dev.* 28, 723–734.
- Sarma, K., Levasseur, P., Aristarkhov, A., and Lee, J.T. (2010). Locked nucleic acids (LNAs) reveal sequence requirements and kinetics of Xist RNA localization to the X chromosome. *Proc. Natl. Acad. Sci. USA* 107, 22196–22201.
- Schindelin, J., Arganda-Carreras, I., Frise, E., Kaynig, V., Longair, M., Pietzsch, T., Preibisch, S., Rueden, C., Saalfeld, S., Schmid, B., et al. (2012). Fiji: an open-source platform for biological-image analysis. *Nat. Methods* 9, 676–682.
- Schoeffner, S., Sengupta, A.K., Kubicek, S., Mechtler, K., Spahn, L., Koseki, H., Jenuwein, T., and Wutz, A. (2006). Recruitment of PRC1 function at the initiation of X inactivation independent of PRC2 and silencing. *EMBO J.* 25, 3110–3122.
- Seibler, J., Zevnik, B., Küter-Luks, B., Andreas, S., Kern, H., Hennek, T., Rode, A., Heimann, C., Faust, N., Kauselmann, G., et al. (2003). Rapid generation of inducible mouse mutants. *Nucleic Acids Res.* 31, e12.
- Sivaguru, M., Urban, M.A., Fried, G., Wessels, C.J., Mander, L., and Punyasena, S.W. (2018). Comparative performance of airyscan and structured illumination superresolution microscopy in the study of the surface texture and 3D shape of pollen. *Microsc. Res. Tech.* 81, 101–114.
- Su, I.H., Basavaraj, A., Krutchinsky, A.N., Hobert, O., Ullrich, A., Chait, B.T., and Tarakhovskiy, A. (2003). Ezh2 controls B cell development through histone H3 methylation and Igh rearrangement. *Nat. Immunol.* 4, 124–131.
- Wang, C.Y., Jégu, T., Chu, H.P., Oh, H.J., and Lee, J.T. (2018). SMCHD1 merges chromosome compartments and assists formation of superstructures on the inactive X. *Cell* 174, 406–421.e25.
- Wutz, A., Rasmussen, T.P., and Jaenisch, R. (2002). Chromosomal silencing and localization are mediated by different domains of Xist RNA. *Nat. Genet.* 30, 167–174.
- Zhao, J., Sun, B.K., Erwin, J.A., Song, J.-J., and Lee, J.T. (2008). Polycomb proteins targeted by a short repeat RNA to the mouse X chromosome. *Science* 322, 750–756.

STAR★METHODS

KEY RESOURCES TABLE

REAGENT or RESOURCE	SOURCE	IDENTIFIER
Antibodies		
α -Smchd1	This study	WEHI in-house Antibody, Monoclonal #8
α -Smchd1	Gdula et al., 2018	Oxford in-house antibody
α -Ciz1	Ridings-Figueroa et al., 2017	University of York, in-house antibody
α -HnmpU	Sigma-Aldrich	Cat # R6278; RRID:AB_477469
α -HnmpK	Abcam	Cat # Ab39975; RRID:AB_732981
α -GFP	Life Technologies	Cat # A-11122; RRID:AB_221569
α -GFP	Abcam	Cat # Ab290; RRID:AB_303395
GFP-Trap_MA	Chromotek	Cat # gtma-400
α -H3K27me3	Millipore	Cat # 07-449; RRID:AB_310624
α -H2AK119ub	Cell Signaling	Cat # 8240; RRID:AB_10891618
α -Ring1B	Active Motif	Cat # 39663
α -Rabbit-IgG	Abcam	Cat # Ab46540; RRID:AB_2614925
α -Rabbit-488	Life Technologies	Cat # A21206; RRID:AB_141708
α -Mouse-555	Life Technologies	Cat # A31570; RRID:AB_2536180
α -Mouse Light Chain	Millipore	Cat # AP200P; RRID:AB_805324
α -Rabbit Light Chain	Millipore	Cat # MAB201P; RRIB:AB_827270
α -Actin-HRP	Santa Cruz	Cat # H1015
Chemicals, Peptides, and Recombinant Proteins		
Recombinant Smchd1 hinge domain protein	Chen et al., 2015	
Critical Commercial Assays		
SMARTer Universal Low Input RNA Kit for sequencing	Clontech	634945
SMARTer Stranded Universal Low Input RNA Kit for sequencing	Clontech	634861
NEBNext Small RNA Library Prep Set for Illumina	New England Biolabs	E7330S
Deposited Data		
PAR-CLIP raw and analyzed data	This study	GEO: GSE119609
Experimental Models: Cell Lines		
B2, B2ΔA and B2ΔB female ES cell lines	G.P., T.N., and N.B., unpublished data	N/A
Primary and immortalized mouse embryonic fibroblasts derived from <i>Smchd1</i> ^{GFP/GFP} strain female embryos	This study	N/A
Primary neural stem cells derived from <i>Smchd1</i> ^{GFP/GFP} female embryos	Jansz et al., 2018	N/A
Primary mouse embryonic fibroblasts derived from <i>Ring1a</i> ^{-/-} ; <i>Ring1b</i> ^{fl/fl} ; <i>Rosa26::CreERT2</i> strain female embryos	Endoh et al., 2008	N/A
Primary mouse embryonic fibroblasts derived from <i>Smchd1</i> ^{GFP/GFP} ; <i>Ezh2</i> ^{fl/fl} female embryos	This study	N/A
Experimental Models: Organisms/Strains		
<i>Smchd1</i> ^{GFP/GFP} mouse strain	Jansz et al., 2018	N/A
<i>Smchd1</i> ^{GFP/GFP} ; <i>Ezh2</i> ^{fl/fl} mouse strain	This study	N/A
<i>Ring1a</i> ^{-/-} ; <i>Ring1b</i> ^{fl/fl} ; <i>Rosa26::CreERT2</i> mouse strain	Endoh et al., 2008	N/A
Oligonucleotides		
shRNA sequences targeting HnmpU, HnmpK, Lbr, Wtap18, Sap18 and Lrif1 and Spen are given in Table S1	This study	N/A
Oligonucleotides for genotyping, cloning and qPCR are given in Table S1	Su et al., 2003 ; Jansz et al., 2018	N/A

(Continued on next page)

Continued

REAGENT or RESOURCE	SOURCE	IDENTIFIER
RNA oligonucleotides for EMSA are given in Table S1	Zhao et al., 2008	N/A
Biotinylated oligonucleotides for iDRIP are given in Table S1	Minajigi et al., 2015	N/A
Oligonucleotides used to amplify Ring1B and mutate Ring1B, given in Table S1	This study	N/A
LNA-scrambled* 5TYE665-GTGTAAACACGTCTATACGCCCA *Position of LNA base was withheld by Exiqon	Sarma et al., 2010 Exiqon	N/A
LNA-4978* 5TYE665-GCTAAATGCACACAGGG *Position of LNA base was withheld by Exiqon	Sarma et al., 2010 Exiqon	N/A
Recombinant DNA		
LMP-BFP with the shRNAs given in Table S1	This study	N/A
MSCV-Cre-puro	This study	N/A
MSCV-Ring1B-puro and MSCV-Ring1B mutant-puro	This study	N/A
LMH with p53 shRNA	Dickins et al., 2005	N/A
pCMV-Xist-PA	Wutz et al., 2002	N/A
Software and Algorithms		
TopHat	Kim et al., 2013	N/A
BWA-PARCLIP	https://github.com/PeteHaitch/bwa-parclip	N/A
PARalyser	Corcoran et al., 2011	N/A
FIJI	Schindelin et al., 2012	N/A
Homer tool analyzeRepeats	Heinz et al., 2010	N/A

CONTACT FOR REAGENT AND RESOURCE SHARING

Further information and requests for resources and reagents should be directed to and will be fulfilled by the Lead Contact, Marnie Blewitt: blewitt@wehi.edu.au

EXPERIMENTAL MODEL AND SUBJECT DETAILS

Animal husbandry and ethics

Smchd1^{GFP/GFP}, *Ezh2*^{fl/fl} and *Smchd1*^{GFP/GFP}; *Ezh2*^{fl/fl} animals were bred at The Walter and Eliza Hall Institute of Medical Research (WEHI), and all procedures performed in accordance with approval AEC 2014.026 then 2018.004, approved by the WEHI animal ethics committee. *Ring1A*^{-/-}; *Ring1B*^{fl/fl}; *Rosa26::CreERT2* mice were bred at Riken, Japan, in accordance with the in-house guidelines for the care and use of laboratory animals of the RIKEN, Yokohama Institute, Japan.

Smchd1^{GFP/GFP} Mice

The *Smchd1*^{GFP} targeted allele was constructed by standard gene targeting techniques using the mouse C1368 ES cell line (129T2/SvEms strain). The 5' (chr17:71,345,341-71,347,443) and 3' (chr17:71,343,347-71,345,340) homology regions for the targeting construct were generated by Pfu polymerase high fidelity PCR. These homology regions were cloned either side of an acGFP ORF (Clontech) and a loxP flanked neo selection cassette so that the acGFP-loxP-neo-loxP cassette was introduced in-frame immediately before the *Smchd1* stop codon. The engineered *Smchd1*^{GFP} allele was designed to produce a fusion protein consisting of wild-type *Smchd1* with a carboxy terminal acGFP moiety. We specifically chose acGFP rather than EGFP because acGFP is known not to dimerize. The targeting construct was introduced into the ES cell line by electroporation. G418 surviving cell clones were screened by Southern blotting of XbaI cut genomic DNA to identify correctly targeted clones. The probe used for Southern blotting was generated by PCR amplification of an upstream genomic region (chr17:71,348,361-71,349,085) that was external to the targeting homology arms but within an XbaI fragment (generated by the XbaI sites at chr17:71,344,994-71,344,999 and chr17:71,349,766-71,349,771) that could be used as diagnostic for correctly targeted clones. Since the targeting construct introduces an XbaI site into the genome, correctly targeted clones were identified by a shift of the usual 4772bp band to a 6691bp band. Correctly targeted ES cell clones were then used for mouse chimera generation by injection of the ES cells into C57Bl6/J strain blastocysts. Once chimeras were identified and germline transmission established, the loxP flanked neo selection cassette was removed by crossing the targeted mice with Cre-deleter mice (E2A-Cre). Crossing of the resulting *Smchd1*^{GFP} allele carrying mice

to homozygosity indicated that the *Smchd1*-acGFP fusion protein was likely to be fully functional since female *Smchd1*^{GFP/GFP} mice were obtained at similar frequencies to *Smchd1*^{+/+} (wild-type) female animals – unlike the loss of function *Smchd1*^{MommeD1} allele which is female embryonic lethal when homozygous. *Smchd1*-GFP localized to the inactive X as has been shown for wild-type *Smchd1* protein. The *Smchd1*^{GFP} allele was backcrossed onto the C57BL/6J strain for 10 generations then maintained as a homozygous congenic line of mice. This strain was genotyped by PCR using oligos specific to the integration site (Table S1).

***Smchd1*^{GFP/GFP}; *Ezh2*^{fl/fl} Mice and MEFs**

Ezh2^{fl/fl} mice were previously described (Su et al., 2003). The *Ezh2*^{fl} allele was backcrossed onto C57BL/6 for more than 10 generations, then bred with C57BL/6 mice carrying the *Smchd1*^{GFP} allele. Compound heterozygous animals were intercrossed and *Smchd1*^{GFP/GFP}; *Ezh2*^{fl/fl} animals bred to create a homozygous line of mice. The *Ezh2*^{fl} and *Ezh2*^{del} alleles were genotyped using oligos given in Table S1.

To conditionally delete *Ezh2* in *Smchd1*^{GFP/GFP}; *Ezh2*^{fl/fl} female primary MEFs, these cells were transduced with a Cre recombinase containing retrovirus, where Cre was cloned into the MSCV-puro backbone (Clontech), to create MSCV-Cre-puro. 24 hours post transduction, 3 µg/mL puromycin was added to the media to select transduced cells. Puromycin was then maintained in the media until analysis, 3-7 days post transduction with Cre.

***Ring1A*^{-/-}; *Ring1B*^{fl/fl}; *Rosa26::CreERT2* Mice and MEFs**

Ring1A null (del Mar Lorente et al., 2000), *Ring1B* floxed (Calés et al., 2008) and *Rosa26::CreERT2* mice (Seibler et al., 2003) were all previously described, as was the generation of the combination together (Endoh et al., 2008).

For conditional deletion of *Ring1B*, *Ring1A*^{-/-}; *Ring1B*^{fl/fl}; *Rosa26::CreERT2* primary female MEFs were treated with 0.8 µM 4OH-tamoxifen, which was refreshed daily for 3 days. Cells were analyzed 1-7 days post induction of Cre.

For the *Ring1B* rescue experiment, *Ring1A*^{-/-}; *Ring1B*^{fl/fl}; *Rosa26::CreERT2* primary female MEFs were treated with 0.8 µM 4OH-tamoxifen as above, or left untreated as controls. The following day MSCV-*Ring1B*-puro and MSCV-*Ring1B* mutant-puro retroviruses were used to transduce the cells. After an additional 24h, transduced cells were selected with 5 µg/mL puromycin. Cells were fixed at day 4 after CreER induction for immunofluorescence, and harvested at day 5 for western blot.

Derivation and culture of Mouse Embryonic Fibroblasts (MEFs)

Female *Smchd1*^{GFP/GFP}, *Smchd1*^{GFP/GFP}; *Ezh2*^{fl/fl} and *Ring1A*^{-/-}; *Ring1B*^{fl/fl}; *Rosa26::CreERT2* MEFs were derived as previously described (Leong et al., 2013). Pregnant females were sacrificed at between 12.5-14.5 days post coitum by cervical dislocation, uterus removed, and embryos removed and washed in PBS (Life Technologies). The embryo tail or yolk sac was taken for genotyping, and the fetal liver, intestines and head removed. The embryo body was disrupted via vigorous pipetting to achieve a near single cell suspension. Cells were cultured in DMEM (GIBCO) with 10% (v/v) FBS (Life Technologies) 37°C in a humidified atmosphere with 5% (v/v) CO₂ and O₂. Cells were maintained by passaging every 3 days using 0.5% trypsin-EDTA (Life Technologies) to detach the cells from the plates, and seeding cells at approximately 3000 cells/cm². The sex of embryos was determined by genotyping for the X-linked genes *Otc* and the Y-linked gene *Zfy*. Oligonucleotides are given in Table S1.

Smchd1^{GFP/GFP} MEFs were immortalized by transduction with retroviral supernatant containing the LMH-p53 construct (LTR-miR30-hygromycin resistance-p53 shRNA) (Dickins et al., 2005). The next day, media was changed, and cells were selected with 500 µg/mL Hygromycin (Roche) for 5 days. Immortalized MEFs were cultured in DMEM (GIBCO) with 10% (v/v) FBS (Life Technologies) 37°C in a humidified atmosphere with 5% (v/v) CO₂ and 20% (v/v) O₂.

Derivation of Neural Stem Cells (NSCs)

NSCs were derived as previously described (Chen et al., 2015). Brains from E14.5 female *Smchd1*^{GFP/GFP} embryos were dissected in Leibovitz's L-15 Medium (Life Technologies). The meninges and subcortical tissue were removed, and forebrains transferred into HBSS (Life Technologies) with 1 mg/mL DNase I (Sigma-Aldrich) and 0.5% trypsin-EDTA (Life Technologies), and incubated at 37°C in 5% (vol/vol) CO₂ for 20 minutes, followed by three washes in HBSS. The tissue was then transferred and mechanically dissociated in NeuroCult NSC Basal Medium (Mouse) (StemCell Technologies) containing NeuroCult Proliferation Supplement (Mouse) (StemCell Technologies), 0.2% heparin solution (StemCell Technologies), 20 ng/mL recombinant human EGF (Peprotech), and 20 ng/mL recombinant human basic FGF (Peprotech). Cells were seeded onto either plates coated with 15 ng/mL polyornithine (Sigma-Aldrich) and 10 ng/mL laminin (Sigma-Aldrich), or directly into tissue culture treated plates with 10 ng/mL laminin (Sigma-Aldrich) added to the medium, at a density of 200,000 cells per cm². Cells were cultured at 37°C in 5% (vol/vol) CO₂ incubator and passaged every 2 days using Accutase (Sigma-Aldrich) to detach the cells from the plates. Primary cells were maintained for a maximum of 20 passages.

***Xist* mutant ES cells**

The generation of female XX ES cells with doxycycline inducible wild-type, A-repeat deletion or B repeat deletion *Xist* transgenes on the X chromosome will be described in detail in another paper that is currently in preparation (G.P., T.N., and N.B., et al., unpublished data). These ES cells were cultured and differentiated according to previous protocols (Penny et al., 1996). ES cell medium consisted of Dulbecco's Modified Eagle Medium (DMEM, Life Technologies) with 20% fetal calf serum (FCS, Seralab), 4.5 g/L glucose, 2mM

L-glutamine, no sodium pyruvate, 1x non-essential amino acids, 0.1 mM 2-mercaptoethanol, 50 g/mL penicillin/streptomycin (all from Life Technologies) and LIF- conditioned medium, made in house, at a concentration equivalent to 1000 U/mL. Pluripotent ES cells were grown on tissue culture dishes coated with PBS + 0.1% gelatin. Cells were grown at 37°C, 5% CO₂ in a humid atmosphere. Cells were passaged using 0.05% trypsin-EDTA (Life Technologies) with 2% Chicken Serum (Life Technologies) and frozen in FCS + 10% DMSO. *Xist* expression driven by TetOn promoter was induced by adding doxycycline (1.5-2 mg/mL) to the culture medium during differentiation. Differentiation was achieved using embryoid body formation, in which cells were plated without LIF for 3 days in hanging drops, then moved to suspension culture for 3 days, then plated as a monolayer on gelatinized tissue culture dishes for 3 days. Cells were analyzed at 9 days of differentiation and *Xist* induction.

METHOD DETAILS

Oligonucleotides and Vectors

21bp siRNA guide strand sequences were designed using dsir. The 21-mer was used to create two complementary 110-mer oligonucleotides with XhoI and EcoRI overhangs for annealing, according to [Dow et al. \(2012\)](#).

shRNA oligonucleotides were cloned into the LMPEBFP2 (LTR miR30 Puromycin IRES EBFP2) or LMPΔGFP vector (LTR miR30 Puro IRES) ([Kinkel et al., 2015](#)). shRNA sequences are given in [Table S1](#).

Long oligonucleotides were annealed with 10 μg of each complementary oligonucleotide, in 50 μL annealing buffer [500 mM potassium acetate, 150 mM HEPES-KOH (pH 7.4), 20 mM magnesium acetate] at 75°C for 5 minutes; 80°C for 10 minutes; 80°C to 55°C stepping down 0.5°C every 2.5 minutes. Products were quantified on the Nanodrop DNA-40 program (Thermo Fisher Scientific), and diluted to 4 ng/μL in H₂O.

Ring1B cDNA was amplified from mouse ES cell cDNA, using oligonucleotides designed to the 5' and 3' ends of the translated sequence, with the addition of XhoI and EcoRI overhangs for cloning (see [Table S1](#)). The amplified cDNA was digested with XhoI and EcoRI, then ligated into MSCV-puromycin (Clontech) that was previously digested with the same two enzymes. The catalytically dead Ring1B (Ring1B mutant) construct was made using the Q5 Site-Directed Mutagenesis Kit (NEB) and the oligonucleotides specified in [Table S1](#), with the MSCV-Ring1B-puro construct as template. Mutagenesis introduced the I53A mutation along with the D56K mutation, both of which are known to remove catalytic activity ([Bentley et al., 2011](#); [Buchwald et al., 2006](#); [Elderkin et al., 2007](#)). The combination of these two mutations together is the subject of a separate manuscript (N. Blackledge and R. Klose, personal communication).

Ligation

Ligation reactions consisted of 1 μL insert prepared above, 100 ng XhoI/EcoRI cut LMPEBFP2 vector, 3 U of T4 DNA ligase (Promega) in 1 X T4 ligase buffer (Promega), 10 μL final volume. Ligations were performed at 16°C overnight.

Transformation

5 μL ligation reaction was added to 50 μL thawed *Escherichia coli* DH10B electrocompetent cells (Life Technologies), transferred to a cuvette and electroporated (2.5kV) using a Micropulser Electroporator (Biorad). 200 μL Superbroth [3.5% (w/v) tryptone, 2.0% (w/v) yeast extract, 0.5% (w/v) NaCl, 5 mM NaOH] was added to the cells before being grown on LG agar plates with 200 μg/mL Carbenicillin (Sigma-Aldrich) overnight.

Plasmid Preparation

1.5mL Superbroth with 200 μg/mL Carbenicillin was inoculated with single colonies from above and incubated overnight at 37°C with shaking. Plasmids were prepared using the Nucleospin Plasmid DNA Purification Kit (Macherey-Nagel), as per manufacturers' instructions. 5 μL plasmid DNA was digested with 10 U EcoRI, 10 U XhoI in 1 X NEB Buffer 4 (New England Biolabs) for 4 hours at 37°C, and run on a 2% (w/v) agarose-TAE gel to verify presence of an insert.

Sequencing Plasmids

Sequencing reaction mix consisted of 1 μL Big Dye v3.1, 1X sequencing buffer (Life Technologies), 250 ng plasmid DNA, 2 μL of 0.8 μM primer, 1X Q solution (QIAGEN), and H₂O to 10 μL. PCR conditions were 96°C for 2 minutes; 30 cycles of 96°C for 10 s, and 60°C for 4 minutes 5 s. DNA was precipitated using 1 volume 3M sodium acetate, 5.5 volumes 100% (v/v) ethanol, 3.5 volumes H₂O, 15 minutes at 4°C and DNA pelleted by centrifugation at 14,600 rpm, 20 minutes. Pellets were washed with 70% (v/v) ethanol, dried at 37°C for 45 minutes and sent to Micromon DNA Sequencing Facility (Monash University, Melbourne).

Retrovirus Production

Retrovirus was prepared as previously described ([Majewski et al., 2008](#)). 293T cells were cultured in DMEM (Life Technologies) supplemented with 10% FBS at 37°C in a humidified atmosphere with 10% (v/v) CO₂. Retroviral supernatants were produced using calcium phosphate mediated transient transfection of 293T cells. 24 hours after plating, 293T cells at 80% confluence were transfected with the MD1-gag-pol structural vector, CAG-Eco or VSVg envelope vector, and shRNA retroviral construct, in the ratio 8:24:1. Plasmid DNA was made up in 250 mM CaCl₂, precipitated in 1 volume 2X HBS solution, and then added to 293T cells in

media containing 25 μ M chloroquine (Sigma-Aldrich). 8 and 24 hours post-transfection, the media was changed. 48 and 72 hours post-transfection, the media was collected, centrifuged to remove residual 293T cells, and either snap frozen or concentrated using Poly(ethylene glycol) (PEG).

Concentration of Retrovirus with PEG

Retroviral supernatant was added to 1/5 volume of 20% PEG solution pH 7.2 [20% Poly(ethylene glycol), 410 mM NaCl] and mixing by inversion 5 times over 90 minutes, followed by incubation at 4°C for 16 hours. Retroviral supernatant was then centrifuged at 4500 rpm for 45 minutes at 4°C, supernatant removed, and retrovirus resuspended in 1/100 original volume of target cells media, before being snap frozen and stored at –80°C.

Transduction of MEFs

MEFs were seeded 4–16 hours prior to transduction. When cells were at 50% confluence a 1:10 dilution of retroviral supernatant was added in media containing 4 μ g/mL polybrene (Sigma-Aldrich). 24 hours later, media was changed and 5 μ g/mL puromycin (Sigma-Aldrich) added for selection for at least 2 days.

Transduction of NSCs

NSCs were seeded at a density of 40,000 cells per cm² 8–16 hours before transduction. PEG concentrated viral supernatant was added to the culture together with polybrene at a final concentration of 4 μ g/mL. On the next day, cells were selected with 1 μ g/mL puromycin.

RNA Extraction

RNA extraction was performed using RNeasy Minikit (QIAGEN) or Quick RNA Kit (Zymo). Cultured cells at 90%–100% confluence were harvested, washed in PBS and RNA extracted as per manufacturers' instructions.

Reverse Transcription of RNA

RNA generated above was quantified using the Nanodrop RNA-40 program. cDNA was generated from 1 μ g of total RNA using 500 ng Oligo(dT)₁₅ (Promega) and 200 U Superscript III Reverse Transcriptase (Life Technologies) as per manufacturer's instructions.

RT-qPCR

3 μ L of 1/30 diluted cDNA was used in a 10 μ L PCR reaction. All assays were performed in triplicate, and standard curves were produced for all assays. UPL Reaction mixes contained 0.2 μ M F and R primers, 0.1 μ M appropriate UPL probe (Roche), and 1X LightCycler® 480 Probes Master Mix (Roche). PCR reactions were performed using LightCycler® 480 Real-Time PCR instrument, with cycle conditions of 95°C for 10 mins; 45 cycles of 95°C for 10 s, 60°C for 30 s; 40°C for 30 s. SYBR Green Reaction mixes contained 0.5 μ M F and R primers, and 1X LightCycler® 480 SYBR Green I Master Mix (Roche). PCR reactions were performed using LightCycler® 480 Real-Time PCR instrument, with cycle conditions of 95°C 5 minutes; 40 cycles of 95°C for 10 s, 60°C for 20 s, 72°C for 20 s; a melt curve was generated at 95°C for 5 s, 65°C for 1 minute, 97°C with Continuous Acquisition (5 per °C); 40°C for 10 s. Cycle thresholds (Ct) were calculated using LightCycler® 480 software and relative mRNA expression levels were calculated using the standard curve method, using *Hmbs* mRNA expression as a control for variation in cDNA concentration between samples (Larionov et al., 2005). Oligonucleotide sequences for the PCRs are given in Table S1.

Live Cell Imaging

Immortalized *Smchd1*^{GFP/GFP} MEFs were transfected with locked nucleic acid (LNA) oligonucleotides containing either a scrambled sequence (Scr) or a sequence targeting *Xist* (Sarma et al., 2010) with a 5' TYE7-5 label (Exiqon). 10⁴ cells were seeded in a 96-well imaging plate (Falcon). After 16 hours, cells were incubated in Opti-MEM media (GIBCO) containing 500 nm LNA probe, 1.5 μ M Lipofectamine 2000 Transfection Reagent (Life Technologies), and 1.5 μ M Lipofectamine Plus Reagent (Life Technologies) for 1 hour. Cells were transferred into DMEM^{GFP} imaging medium (Evrogen) and fluorescent images were captured every 10 minutes over 12 hours using a Plan-Apochromat 20X/0.8 Zeiss objective on the Zeiss Live Cell Observer and captured using an AxioCam MRm CCD camera. Cells were maintained in a humidified atmosphere with 10% CO₂ at 37°C. Images were analyzed manually using the open source ImageJ distribution package, FIJI (Schindelin et al., 2012).

Immunofluorescence

Immunofluorescence on *Smchd1*^{GFP/GFP}, *Smchd1*^{GFP/GFP}; *Ezh2*^{fl/fl}, *Smchd1*^{GFP/GFP}; *Ezh2*^{del/del}, *Ring1A*^{–/–}; *Ring1B*^{fl/fl}, *Rosa26::CreERT2* and *Ring1A*^{–/–}; *Ring1B*^{del/del}, *Rosa26::CreERT2* MEFs and *Smchd1*^{GFP/GFP} NSCs, or B2, D2ΔA and B3ΔB cells at day 9 of differentiation, was performed as described in Chaumeil et al. (2008), with modifications. Cells were seeded at 70% confluence the night before the experiment on either gelatin (MEFs) or polyornithine and laminin (NSCs) coated chamber slides. The next day, cells were washed in PBS, and fixed in 3% (w/v) paraformaldehyde made in PBS for 10 minutes at room temperature. Cells were washed three times in PBS for 5 minutes each, and then permeabilised in cold 0.5% (v/v) Triton X-100 in PBS on ice for 5 minutes. Cells were washed three times in PBS for 5 minutes each, and then blocked in 1% (w/v) Bovine Serum Albumin

(BSA) (Life Technologies) for at least 15 minutes. Cells were then incubated with a primary antibody diluted in 1% (w/v) BSA for 45 minutes at room temperature in a humid chamber. Cells were washed three times in PBS for 5 minutes each, and then incubated with a secondary antibody conjugated to a fluorophore diluted in 1% (w/v) BSA for 40 minutes at room temperature in a dark and humid chamber. Cells were washed three times in PBS for 5 minutes each, and were mounted in Vectashield HardSet mounting medium with DAPI (Vector Laboratories). When *Smchd1*^{GFP/GFP} cells were used, detection of Smchd1 protein was enabled via detection of native Smchd1-GFP fusion protein. Cells were visualized on an Elite Widefield (DeltaVision), LSM 880 (Zeiss), or Live-Cell AxioObserver (Zeiss) microscope. Images were analyzed using the open source ImageJ distribution package, FIJI (Schindelin et al., 2012).

Xist RNA FISH

Xist RNA FISH was performed on *Smchd1*^{GFP/GFP} MEFs or differentiating ES cells as described (Chaumeil et al., 2008), with modifications. Briefly, Xist RNA was detected with the 15 kb cDNA, pCMV-Xist-PA, as described (Wutz et al., 2002). 2 µg Xist cDNA was used in a nick translation reaction (Vysis) to generate DNA probes labeled with SpectrumRed dUTP (Vysis). ~100 ng probe per sample was precipitated in Ethanol with 10% NaOAc, and 1 µg Salmon Sperm (Life Technologies), before being resuspended in formamide (Sigma-Aldrich), and denatured at 75°C for 10 minutes. Denatured probe was kept on ice for a maximum of 30 minutes while cells were being prepared. Cells were seeded at 70% confluence the night before the experiment on either gelatin (MEFs) or polyornithine and laminin (NSCs) coated glass coverslips. The next day, coverslips were washed in PBS, and cells were fixed in 3% (w/v) paraformaldehyde made in PBS for 10 minutes at room temperature. Coverslips were washed three times in PBS for 5 minutes each, and then cells were permeabilised in cold 0.5% (v/v) Triton X-100 in PBS containing 2 mM Ribonucleoside Vanadyl Complexon (RVC) (New England Biolabs) on ice for 5 minutes. Coverslips were washed three times in 70% (v/v) Ethanol for 5 minutes, and then cells were dehydrated by sequential 3 minute washes in 80%, 95% and 100% Ethanol. Coverslips were then placed upside down on denatured probe in formamide added to an equal volume of 2 X Hybridization buffer [4 × SSC (Sigma-Aldrich), 40% w/v dextran sulfate (Sigma-Aldrich), 2 mg/mL BSA (New England Biolabs), and 400 mM RVC]. Hybridization occurred overnight at 37°C in a dark chamber humidified with 50% formamide, 50% 2 X SSC. The next morning coverslips were washed three times 50% formamide, 50% 2 X SSC at 42°C, followed by three times in 2 X SSC at 42°C. Coverslips were mounted in Vectashield HardSet mounting medium with DAPI (Vector Laboratories). Cells were visualized on an Elite Widefield (DeltaVision), LSM 880 (Zeiss), or Live-Cell AxioObserver (Zeiss) microscope, with Airyscan processing. Images were analyzed using the open source ImageJ distribution package, FIJI (Schindelin et al., 2012).

To determine overlap between Smchd1 and Ring1B, HnrnpK, HnrnpU or H2AK119ub the CoLoc2 package was used in FIJI. Background subtracting was performed using a rolling ball algorithm set to a radius of 5. The region of interest was defined as the inactive X chromosome, based on focal Smchd1 enrichment. Pearson's correlation were calculated for all pixels on each channel above automatically determined threshold values. To calculate percent overlap, a binary mask was generated for each channel above threshold values generated by Coloc2 analysis, and was used to calculate the percentage of area where colocalization is present.

GFP Immunofluorescence and Xist RNA FISH

To perform immunofluorescence and RNA FISH in combination, the immunofluorescence protocol was followed as above. Following incubation with the secondary antibody, and three 5 minute PBS washes, coverslips were post-fixed in 3% PFA at room temperature for 10 minutes. Coverslips were washed twice in 2 X SSC for 5 minutes, and then RNA FISH protocol was followed as above, from the hybridization step on. Cells were visualized on an LSM 880 (Zeiss) microscope, with an Airyscan detector. Images were analyzed using the open source ImageJ distribution package, FIJI (Schindelin et al., 2012).

3D SIM

Super-resolution 3D-SIM was performed on a DeltaVision OMX V3 Blaze system (GE Healthcare) equipped with a 60x/1.42 N.A. Plan/Apo oil immersion objective (Olympus), sCMOS cameras (PCO), and 405, 488 and 568 nm lasers, and 1.518 refractive index immersion oil. 3D-SIM image stacks were acquired using recommended settings; 15 raw images per plane (5 phases, 3 angles) and a z-step size of 125nm. Data reconstruction and color channel alignment were performed with SoftWoRx 6.1 (GE Healthcare) using channel-specific optical transfer functions (OTFs) and Wiener filter settings 0.0010. All 3D-SIM data was evaluated via SIMcheck, an open-source ImageJ plugin to assess SIM image quality (Ball et al., 2015).

Preparation of Whole Cell Extract and Fractionation

3x10⁶ *Smchd1*^{GFP/GFP} or *Smchd1*^{+/+} MEFs were treated with trypsin-EDTA and washed twice in cold MTPBS. The following steps were all performed with rotation at 4°C for 10 minutes, followed by centrifugation at 13,000rpm at 4°C for 5 minutes. Cells were lysed with 500 µL KALB lysis buffer [150 mM NaCl, 50mM Tris-HCl (pH 7.5), 1% (vol/vol) Triton X-100, 1 mM EDTA (pH 7.5)] supplemented with 1 X cComplete protease inhibitor (Roche), 2 mM Na3VO4 and 1 mM PMSF, and supernatant was collected as whole cell extract. Pellet was treated with 20 µg/mL DNase I (Sigma-Aldrich) in 10 mM Tris pH 7.5, 2.5 mM MgCl₂ and 500 µM CaCl₂. Supernatant was collected as DNase fraction, and pellet was treated with Benzonase (Sigma-Aldrich) in 10 mM Tris pH 8, 2 mM MgCl₂ and 20 mM NaCl. Supernatant was collected as Benzonase fraction, pellet was treated with Benzonase in 10mM Tris pH 8, 2 mM MgCl₂, 300 mM NaCl, and 0.05% Igepal CA-630 (Sigma-Aldrich). Supernatant was taken as high-salt Benzonase fraction, and pellet was boiled in 1 X Laemmli buffer [2% (wv) SDS, 10% (v/v) glycerol, 60 mM Tris-HCl (pH 6.8), 0.01% (w/v) bromophenol blue].

Protein Quantification

Protein concentration was quantified using a Pierce BCA Protein Assay Kit (Thermo Fisher Scientific). 10 μ L whole cell extract and 0.1–10 mg/mL BSA standards were added to 100 μ L working solution in duplicate. Assay was incubated at 37°C for 30 minutes. Protein concentration was determined by absorbance at 570 nm on Multiskan Ascent plate reader, and calculated against standards.

Silver Stain

Proteins were resolved by reducing SDS-PAGE on 4%–12% Bis-Tris gels (Novex) in MES buffer (Life Technologies). Gel was fixed with 30% ethanol and 10% acetic acid for 30 minutes, and then 2% (v/v) glutaldehyde, 0.2% (w/v) $\text{Na}_2\text{S}_2\text{O}_3$, 30% EtOH, and 0.4M NaAc pH 6 for 90 minutes at room temperature. Gel was then washed 3 times for 30 minutes each at room temperature. Gel was stained in a solution of 0.1% (w/v) AgNO_3 and 0.02% (w/v) formaldehyde for 30 minutes at room temperature, and then developed with 2.5% (w/v) Na_2CO_3 and 0.01% (w/v) formaldehyde until signal was detected. Gel was washed with MilliQ H_2O three times and developing reaction quenched in 12% (v/v) MeOH and 7% (v/v) Acetic acid.

Western Blot

Proteins were resolved by reducing SDS-PAGE on 4%–12% Bis-Tris gels (Novex) in MES buffer (Life Technologies), and transferred to a PVDF membrane by wet transfer for 1 hour at 100V. Membranes were blocked in 5% (w/v) skim milk powder in 0.1% Tween-20/PBS for 1 hour at room temperature. The membrane was probed with a primary antibody in blocking solution overnight at 4°C or for 1 hour at room temperature, washed over 30 minutes with 0.1% Tween-20/MTPBS (6 changes), incubated with the appropriate secondary antibody conjugated to HRP in blocking solution for 1 hour, and rinsed as above. Antibody binding was visualized using the Luminata ECL system (Millipore) following the manufacturer's instructions.

Immunoprecipitation

400 μ L of whole cell extract was incubated with 5 μ g antibody at 4°C for 2 hours with rotation. The lysate-antibody mix was incubated with 20 μ L pre-washed Dynabeads Protein G (Life Technologies) for 1 hour at 4°C. Tubes were placed on a magnetic stand, and unbound supernatant was collected. Beads were washed with 500 μ L KALB lysis buffer 5 times, and the immuno-complex was eluted from the beads with 40 μ L 2X Laemmli buffer. Input, elution and IgG control were analyzed by SDS-PAGE and western blot as above.

PAR-CLIP

PAR-CLIP was performed as described, with modifications (Hafner et al., 2010). In brief, 2×10^9 female *Smchd1*^{GFP/GFP} and *Smchd1*^{+/-} were incubated with 100 μ M 4-thiouridine (Sigma-Aldrich) for 16 hours. 10^9 cells were then irradiated with 150 mJ/cm² UV light at 365 nm, and 10^9 cells were kept aside as a no-crosslink control. Cells were washed in cold PBS, scraped, and lysed in 3 volumes of cold lysis buffer [50 mM HEPES (pH 7.5), 150 mM KCl, 2mM EDTA, 0.5% Igepal CA-630, 0.5 mM DTT, 1 X cOmplete protease inhibitor (Roche)] and nuclei disrupted by passing lysate through a 30G syringe 10 times. Lysate was treated with 30 U Turbo DNase (Life Technologies) at 37°C for 15 minutes with rotation. Lysate was cleared by centrifugation at 13000 x g for 15 minutes at 4°C. 1 U/ μ L RNase T1 (Life Technologies) was added to lysate and incubated at 22°C for 15 minutes, then samples were placed on ice for 5 minutes. 1 volume of lysis buffer without Igepal CA-630 (wash buffer) was added to each sample to achieve a final concentration of 0.25% Igepal CA-630. 125 μ L GFP-TRAP_M beads (ChromoTek) was added to each sample for 2 hours, with rotation at 4°C. Beads were washed three times in wash buffer, and were resuspended in 100 μ L dephosphorylation buffer [50mM Tris pH7.5, 100 mM NaCl, 10 mM MgCl_2 , 1mM DTT] containing 0.5 U/ μ L calf intestinal alkaline phosphatase (New England Biolabs) and incubated at 37°C for 10 minutes. Beads were washed twice in phosphatase wash buffer [50mM Tris pH 7.5, 20 mM EGTA, 0.5% Igepal CA-630] and twice in Polynucleotide Kinase Buffer (PNK buffer) [50 mM Tris pH 7.5, 50 mM NaCl, 10 mM MgCl_2 , before being resuspended in PNK containing 0.5 μ Ci/ μ L γ -³²P-ATP and 0.8 U/ μ L T4 PNK (New England Biolabs) and incubated at 37°C for 30 minutes. 100 μ M dATP was added, and samples were incubated for 5 minutes at 37°C. Beads were washed 5 times in PNK buffer, and boiled in 2 X Laemmli buffer. RNPs were resolved by reducing 4%–12% Bis-Tris SDS-PAGE with MES running buffer, and gel was exposed to Amersham Hyperfilm (GE Life Sciences) overnight. Developed film was aligned with gel, and a band at 250 kDa corresponding to the size of Smchd1-GFP was cut from each sample. RNPs were electroeluted from the gel in a D-Tube Dialyzer Midi (Merck) in MOPS running buffer. Samples were incubated at 55°C for 30 minutes with the addition of 1.2 mg/mL Proteinase K (Roche), 3 mM CaCl₂, and 1% SDS. RNA was then extracted using miRNeasy Micro Kit (QIAGEN) as per manufacturers instructions. Libraries were made using SMARTer Universal Low Input RNA Kit for sequencing (Clontech), SMARTer Universal Low Input Stranded RNA Kit (Clontech), or NEBNext Small RNA Library Prep Set for Illumina (New England Biolabs).

RNA Immunoprecipitation (RIP)

RIP was performed as previously described (Hasegawa et al., 2010). Briefly, 6×10^6 *Smchd1*^{GFP/GFP} MEFs were irradiated with 254 nm UV light at 400 mJ/cm², washed in cold PBS, scraped, and lysed in 200 μ L SDS buffer [50 mM Tris-HCl, 150 mM NaCl, 1 mM EDTA, 1 mM DTT, 1% (w/v) SDS, 1% (v/v) Triton X-100] on ice for 10 minutes. Lysate was subject to sonication using the Covaris S220. 800 μ L dilution buffer [50 mM Tris-HCl, 150 mM NaCl, 1 mM EDTA, 1% (v/v) Triton X-100] was added to sonicated sample containing 1 X cOmplete protease inhibitor (Roche) and 400 U/mL SuperIn RNase Inhibitor (Life Technologies). Lysate was cleared by centrifugation at 13000 x g for 15 minutes at 4°C. 10% lysate was taken for input. 5 μ g antibody or IgG control

was added to the remaining lysate and incubated for 2 hours with rotation at 4°C. The lysate-antibody mix was incubated with 20 μ L pre-washed Dynabeads Protein G (Life Technologies) for 1 hour at 4°C. Tubes were placed on a magnetic stand, and unbound supernatant was collected. Beads were washed twice with 500 μ L Wash Buffer 1 [20 mM Tris-HCl (pH 8.0), 500 mM NaCl, 1 mM EDTA, 0.1% SDS, 1% Triton X-100] and then three times with 500 μ L Wash Buffer 2 [20 mM Tris-HCl (pH 8.0), 150 mM NaCl, 1 mM EDTA, 0.1% SDS, 1% Triton X-100]. The immuno-complex was eluted from the beads by Protease K treatment; both the beads and input were incubated with 200 ng/ μ L Proteinase K (Roche) in 10 mM Tris and 1 mM EDTA containing 0.5% (w/v) SDS for 1 hour at 37°C. RNA was then extracted using Trizol-LS (Life Technologies) as per manufacturer's instructions, and cDNA was made for using 10 μ L of input or co-immunoprecipitated RNA for RT-qPCR.

An alternative RIP protocol was performed as PAR-CLIP was, but with the following modifications. 10⁶ *Smchd1*^{GFP/GFP} MEFs were irradiated with 254 nm UV light, washed in cold PBS, scraped, and lysed in 3 volumes of cold lysis buffer, and nuclei disrupted by passing lysate through a 23G syringe 10 times. Lysate was treated with 30 U Turbo DNase (Life Technologies) at 37°C for 15 minutes with rotation. Lysate was cleared by centrifugation at 13000 x g for 15 minutes at 4°C. 1 volume of wash buffer was added to each sample, and 20 μ L GFP-TRAP_M beads (ChromoTek) was added and incubated for 2 hours with rotation at 4°C. Beads were washed three times in wash buffer, then incubated at 55°C for 30 minutes in the presence of 1.2 mg/mL Proteinase K (Roche), 3 mM CaCl₂, and 1% SDS. RNA was then extracted using Trizol-LS (Life Technologies) as per manufacturer's instructions. cDNA was made for using 10 μ L of input or co-immunoprecipitated RNA for RT-qPCR.

Identification of Direct RNA interacting Proteins (iDRIP)

iDRIP was performed as described (Minajigi et al., 2015), with modifications. Approximately 5 × 10⁷ male and female *Smchd1*^{GFP/GFP} NSCs, incubated in the presence (+ve) or absence (-ve) of 4-thiouridine (4-SU, Sigma) for 16 hours were irradiated with 200 mJ UV light at 254 nm (4-SU -ve) 150 mJ UV light at 356 nm (4-SU +ve). Cells were lysed, and DNase treated as published, while biotinylated probes antisense to *Xist* were conjugated to MyOne C1 Streptavidin Beads (Thermo Scientific). Beads were washed twice in wash buffer [100 mM NaOH and 50 mM NaCl] and once in 100 mM NaCl, before being added to 100 pmol *Xist* probe cocktail in 10 mM Tris pH 7.5, 1 mM EDTA, and 2 M NaCl, and incubated for 10 minutes. Probe-bead conjugates were washed in wash buffer, and resuspended in 10 mM Tris and 1 mM EDTA. 10% lysate was taken as WCE. Hybridization of lysate to probes was done overnight with a temperature gradient of 55°C to 37°C with rotation. Washes were performed at 37°C, 5% enriched material was taken for RNA extraction in Trizol (Life Technologies), and from the remaining material, proteins were eluted from the beads by boiling in 40 μ L 2 X SDS buffer. Samples were resolved via Western Blot. Oligonucleotide sequences for *Xist* pulldown are given in Table S1.

Recombinant Protein Expression

Constructs used for protein expression were described in Chen et al. (2015), and oligonucleotides for amplification of the hinge domain are given in Table S1. Recombinant proteins were expressed and purified from BL21-CodonPlus expression competent *Escherichia coli* cells (Agilent). Cells were cultured in Superbroth with 100 μ g/mL ampicillin to an A600 of ~0.6–0.8 before inducing expression with 0.5 mM isopropyl b-D-1-thiogalactopyranoside (IPTG) for 16 hours at 18°C. Purification was performed as described @Babon:2013ec. Briefly, cells were lysed in lysis buffer [0.5 M NaCl, 20 mM Tris (pH 8), 20% (vol/vol) glycerol, 5 mM imidazole (pH 8), 0.5 mM Tris (2-carboxyethyl)phosphine], supplemented with 1 mM PMSF, by sonication and debris removed by centrifugation. N-terminal 6-His-tagged proteins were purified by nickel-nitrilotriacetic acid (Ni-NTA) FastFlow resin (QIAGEN), washed with 35 mM imidazole (pH 8.0) buffer, and eluted in lysis buffer with 250 mM imidazole (pH 8). The tag was cleaved by incubation with tobacco etch virus (TEV) protease for 1 hour at room temperature. Cleaved protein was concentrated with a 30-kDa molecular mass cutoff concentrator (Millipore) at 4°C by centrifugation at 3300 x g and then diluted with the lysis buffer. Subtractive Ni-NTA chromatography with the resin was performed to eliminate undigested protein and TEV protease, followed by a final Superdex-200 10/300 GL gel filtration (GE Healthcare) in 100 mM NaCl and 20 mM HEPES (pH 7.5). Fractions containing the *Smchd1* hinge domain were pooled, concentrated, aliquoted and snap-frozen in liquid nitrogen for storage at –80°C.

EMSAs

6-FAM labeled RNA oligonucleotides (50 nM) were mixed with the recombinant *Smchd1* hinge domain (WT or R1867G mutant) in a 0-, 10-, 50-, 250-, and 1,000-fold molar excess over the RNA oligonucleotides in PBS in a total volume of 20 μ L. After incubation at room temperature for 30 minutes, 5 μ L of 50% (vol/vol) glycerol was added to the samples. Samples were loaded onto a 0.5% (wt/vol) agarose gel in 1 × Tris base, boric acid, EDTA (TBE) buffer and separated for 1.5 hours at 4 V/cm at 4°C. Gels were scanned on a Typhoon 9410 fluorescence scanner with 526-nm short-pass filter (GE Healthcare). RNA oligonucleotide sequences are given in Table S1.

QUANTIFICATION AND STATISTICAL ANALYSIS

All statistical information pertaining to the number of replicates and significance can be found in the figure legends. All experiments were performed on n = 3 where possible, to ensure reproducibility while being affordable. Instances where n < 3 were due to limited availability of primary cell lines or reagents, or because independent techniques were used to validate findings where n = 2. When n < 3 it is indicated in the figure legend. It was not appropriate to randomize samples, as specific genotypes were required. Additional

statistical information for the PAR-CLIP experiments can be found in the results section. Specific information for each experiment are detailed in each subsection below.

T-Tests for Imaging and Knockdown Data

P values to define significance for all imaging and shRNA knockdown data were determined using unpaired students 2 tailed t tests in GraphPad Prism, or paired t tests in the case of *Ezh2*^{fl/fl} and *Ezh2*^{del/del} samples. In all instances n represents experiments performed on independent cell lines. All percentages displayed represent the mean \pm SEM. In each experiment a minimum of 50 cells were scored in at least two biological replicates, unless otherwise indicated.

PAR-CLIP

PAR-CLIP was performed in two independent NSC cell lines (n = 2), each in technical duplicates, thus generating 4 datasets for analysis from n = 2. Libraries were sequenced on Illumina NextSeq platform, using 75bp, single-end reads. We obtained 20-60 million reads for each sample, but as few as 1 million for negative controls. Adapters were trimmed from reads using TrimGalore. We employed two strategies to align our data: BWA-PARCLIP, a modified BWA alignment tool to be able to map the C-T transitions generated by PAR-CLIP (<https://github.com/PeteHaitch/bwa-parclip>); and TopHat with the following options (-read mismatches 5-read-edit-dist 5) (Kim et al., 2013). We achieved a mapping efficiency of 21%. The majority of the PAR-CLIP tags were distributed between protein coding and repetitive transcripts (37.2% and 38.2% respectively), with intergenic and annotated non-coding transcripts accounting for 18.8 and 5.8% tags respectively.

Clusters were called running PARalyzer using the default parameters, identifying 4763 peaks across the genome (p < 0.05) (Corcoran et al., 2011). Sequencing data were analyzed using Seqmonk v1.36.1, by quantifying reads under PARalyzer clusters, normalized for library size using Match normalization. Normalized *Smchd1*^{+/+} or No-Crosslink control reads were subtracted from *Smchd1*^{GFP/GFP} reads under PARalyzer clusters, identifying 9 specific clusters that were enriched two-fold over background reads genome-wide. Analysis of repeats was performed using the Homer tool analyzeRepeats.pl with the following parameters (repeats mm10) (Heinz et al., 2010).

Colocalisation Analyses

For all colocalization analyses, n represents independent cell lines. Percentages reported are the mean \pm SEM. Analyses were performed in at least two independent cell lines. To determine overlap between *Smchd1* and *Xist*, the CoLoc2 package was used in FIJI. Background subtracting was performed using a rolling ball algorithm set to a radius of 5. The region of interest was defined as the inactive X chromosome, based on focal *Smchd1* enrichment. Pearson's correlations were calculated for all pixels on each channel above automatically determined threshold values. To calculate percent overlap, a binary mask was generated for each channel above threshold values generated by Coloc2 analysis, and was used to calculate the percentage of area where colocalization is present.

To determine percent colocalization between *Smchd1* and Ring1B or H2AK119ub, the Xi was defined based on focal *Smchd1* enrichment. A binary mask was generated for each channel using the Li Dark method to auto-threshold 16-bit images. The masked images were then used to determine percentage of the Xi occupied on each channel. Percentage of area where colocalization occurred was generated by Coloc2 analysis using the signal above threshold values.

DATA AND SOFTWARE AVAILABILITY

The accession number for the PAR-CLIP datasets reported in this paper is GEO: GSE119609.